Beam Simulation of a Prototype Proton Electric Dipole Moment Storage Ring

Master Thesis

OF

Saad Siddique

submitted to

Faculty: Mathematics, Computer Science and Natural Science
of the RWTH Aachen University
on
Dated: - -
carried out at the
Physics Institute III B
under
Prof. Dr. Andreas Lehrach

Abstract

The matter-antimatter asymmetry may be explained through CP-violation by observing a permanent electric dipole moment (EDM) of subatomic particles. An advanced approach to measure the EDM of charged particles is to apply a unique method of "Frozen spin" on a polarized beam in an accelerator. To increase the experimental precision step by step and to study systematic effects, the EDM experiment can be performed within three stages: the magnetic ring COSY[1], a prototype EDM ring and finally all electric EDM ring. The intermediate ring will be a mock-up of the final ring, which will be used to study a variety of systematic effects and the main principle of the final ring. In this thesis, simulations towards the optics of the prototype ring are performed and discussed. The lattice optics with different focusing strengths are generated and studied. Estimations of beam losses in the prototype ring for different lattices are performed by using analytical formulas. These tasks are performed, to minimize systematic errors and enhance beam lifetime in the ring, by optimizing lattice.

[1]COOler SYnchrotron storage ring at Forschungszentrum Jülich

Contents

CHAPTER 1

Introduction

Explaning the baryogenesis is one of the major challenges for modern physics. The matter-antimatter asymmetry riddle may be solved by observing a permanent existance of the Electric Dipole Moments (EDM) of subatomic particles.

The Standard Model of particle physics predicts non-vanishing EDMs but their magnitude is too small to explain the baryogenesis with current techniques. However, the existance of permanent EDMs is only possible through charge and parity (CP) symmetry violation [1]. In the past, most of the EDM measurements were performed for neutral particle systems. But now dedicated measurements of the EDM for charged hadrons are also possible at storage rings where polarized beams can be obtained.

The Jülich Electric Dipole moment Investigations (JEDI[1]) collaboration at the Institute of Nuclear Physics of the Forschungszentrum Jülich is working on the investigation of EDMs of protons and deutrons. The future plan of JEDI is to measure the EDM of charged particles in a storage ring under the influence of electromagnetic fields with the help of new technique called "Frozen Spin". This technique demands to align the polarization parallel to particles longitudinal momentum, thus vertical polarization build up gives a clue to measure EDM. The purposed storage ring is to measure the EDM of the proton with all electric elements for ultimate precision. However, this ring follows two stages (Precursor experiment at COSY and Prototype proton storage ring) to reduce systematic effects and increase the EDM measurement precision. One of the possible ways to reduce systematic effects is the use of counter-rotating beams simultaneously in an all electric ring.

In this thesis, the next chapter briefly describes the scientific reasoning for the measurements of EDMs through an accelerator machine. It also explains the method of "Frozen spin" to measure the EDMs of protons and deutrons. The third chapter is about a proposed prototype storage ring including a motivation for it. The structure and measurement goals of this prototype ring are explained in the same chapter. There are two tasks of beam simulation for this prototype ring which are performed in this thesis. The first is to study the beam optics which will focus on the generation of four different lat-

[1]an international collaboration

tices with different focusing strengths and the second task is to calculate the beam losses for all lattices to find an optimal lattice. The linear beam dynamics for these tasks are explained in chapter 4. The transfer matrix for electrostatic deflectors is also explained by studying the Hamiltonian. Furthermore, four main factors of beam losses with all necessary formulas are briefly discussed at the end of chapter 4. The fifth chapter is about the beam simulation results which shows four different lattices generated by the Methodical Accelerator Design (MAD-X) [2] program with manual extensions of electric defelectors by introducing matrix elements. Additionally beam losses for major scattering effects are calculated by using Wolfram Mathematica [3]. The four types of lattices with different focusing strengths are studied in detail with distinctive bending matrices followed by beam loss investigations for all four lattices to compare them and to find a conclusive lattice which seems to have desirable balance in between long beam lifetime and less systematic errors.

CHAPTER 2

Electric Dipole Moment Measurement

2.1 Science Context and Objectives

A lot of developments in physics since the last 100 years is by dint of breaking or conserving of symmetry patterns. The expansion of the Standard Model (SM) of particle physics has been relied on experimental attempts of discrete symmetries (*e.g.* parity P, charge conjugation C, their product CP, time-reversal invariance T, the product CPT, baryon- and/or lepton number).

Due to explicit violation of both time-reversal (T) and parity (P) symmetries while the charge symmetry (C) can be maintained, a nonzero permanent electric dipole moment (EDM) for all subatomic particles having nonzero spin (regardless whether of elemenatry or composite nature could exist). Considering the conservation of combined (CPT) symmetry, T-violation also implies CP-violation. The CP-violation generated by the Kobayashi-Maskawa (KM) mechanism of weak interactions contributes a very small EDM value that is several orders of magnitude below to current experimental limits. A non-zero EDM value of any subatomic particle would be a sign that there exists a new source of CP-violation, either induced by the strong Quantum Chromodynamics (QCD) angle θ_{QCD} or by genuine physics beyond the Standard Model (BSM)[4]. The mystery of the observed baryon-antibaryon asymmetry in our universe can also be explained by CP-violation beyond the SM. The quest to improve the experimental bounds of the permanent EDM of the neutron, d_n, has served to rule out or at least to severely constrain many theories of CP violation, demonstrating the power of sensitive null results. The current bound of the neutron EDM resulting from these efforts is

$$|d_n| < 3.0 \times 10^{-26}\,\mathrm{e\,cm}(90\%\mathrm{C.L.})[5] \tag{2.1}$$

The EDMs of many paramagnetic and diamagnetic atoms have been estimated, however for our interest, due to Schiff screening, the indirect bounds on the neutron and proton EDMs obtained by applying nuclear physics methods [6] are much weaker than their parent atom bounds. From the best case of ^{199}Hg, indirect measurements of the neutron and the proton EDMs are [7]

$$|d_n^{\downarrow ^{199}\mathrm{Hg}}| < 1.6 \times 10^{-26}\,\mathrm{e\,cm}(95\%\mathrm{C.L.}),$$

$$|d_p^{\downarrow ^{199}\mathrm{Hg}}| < 2.0 \times 10^{-25}\,\mathrm{e\,cm}(95\%\mathrm{C.L.}),$$

The indirect bound on $|d_p|$ is by a factor of 13 weaker than the indirect $|d_n|$ and therefore not really competitive.

The current status of the already excluded EDM regions [8, 9, 10] derived from the experimental upper limits of the various particles are summarised in Figure 2.1.

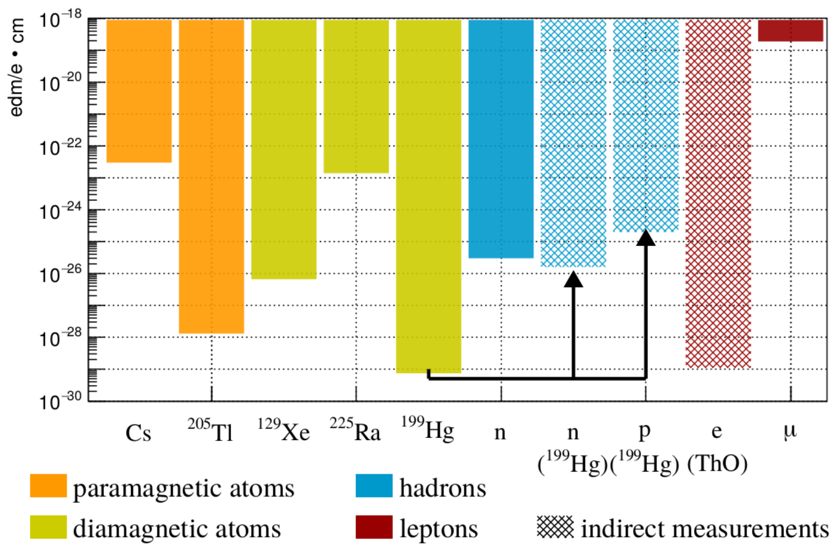

Figure 2.1: Current status of excluded regions of electric dipole moments. Shown are direct and/or derived EDM bounds of the particles[4].

A direct measurement of the EDM of the proton through a storage ring method, would be compareable or better than current investigations of neutron EDM with aim of $|d_n| \sim 10^{-28}\,\mathrm{e\,cm}$ sensitivity with ultra-cold neutrons. The neutron investigations measure the precession frequency jumps in traps containing magnetic and electric fields, when the sign of the electric field is changed. As proton beams trap significantly more particles therefore the statistical sensitivities may reach to the order of $10^{-29}\,\mathrm{e\,cm}$ [4] with the new method using a storage ring under the influence of electric fields. Hence a storage ring could take the lead as the most senstitive method for the discovery of an EDM measurement.

2.2 Method and Strategy

The experimental method to measure an electric dipole moment of fundamental particle or subatomic system often relies on the spin precession rate in an external field. The spin motion can be understood by studying the Thomas-BMT[1] equation in the following section.

2.2.1 Thomas-BMT Equation

The EDM signal is based on the rotation of the electric dipole in the presence of an external electric field that is perpendicular to the particle's spin. The particles are formed into a spin-polarized beam. Measurements are made on the beam as it circulates in the ring, confined by the electromagnetic fields. In the particle frame, an electric field generates pointing towards the center of the ring.

The spin motion of particles in a circular accelerator or storage ring is described by the Thomas-BMT equation and its extension for the EDM [11, 12]

$$\frac{\mathrm{d}\vec{S}}{\mathrm{d}t} = \left(\vec{\Omega}_{\mathrm{MDM}} + \vec{\Omega}_{\mathrm{EDM}}\right) \times \vec{S} \tag{2.2}$$

where

$$\vec{\Omega}_{\mathrm{MDM}} = -\frac{q}{m}\left[G\vec{B} - \frac{\gamma G}{\gamma+1}\vec{\beta}(\vec{\beta}\cdot\vec{B}) - \left(G - \frac{1}{\gamma^2-1}\right)\frac{\vec{\beta}\times\vec{E}}{c}\right] \tag{2.3}$$

$$\vec{\Omega}_{\mathrm{EDM}} = -\frac{\eta q}{2mc}\left[\vec{E} - \frac{\gamma}{\gamma+1}\vec{\beta}(\vec{\beta}\cdot\vec{E}) + c\vec{\beta}\times\vec{B}\right]. \tag{2.4}$$

The angular frequencies, $\vec{\Omega}_{\mathrm{MDM}}$ and $\vec{\Omega}_{\mathrm{EDM}}$, act through the magnetic dipole moment (MDM) and electric dipole moment (EDM) respectively. $\vec{S}$ denotes the spin vector in the lab frame, t is the time in the laboratory system, $\beta = v/c$ and γ are the relativistic Lorentz factors, and B and E are the magnetic and electric fields respectively. G(magnetic anomaly) and η are dimensionless quantities.

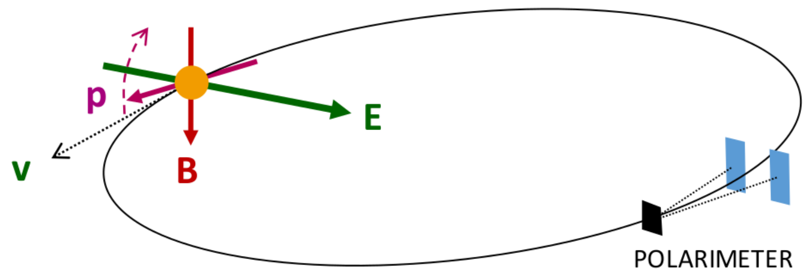

Figure 2.2: Diagram shows a particle motion around the storage ring under the influnence of electromagnetic fields. The polarization, initially along the longitudinal velocity, precesses slowly upward in response to the radial electric field acting on the EDM. The vertical component of the polarization is observed through scattering in the polarimeter [4].

[1]The Thomas-Bargmann-Michel-Telegdi(Thomas-BMT) equation

The effect of the torque is shown in Fig 2.2 where $\vec{v}$ is the particle velocity along the orbit, $\vec{B}$ and $\vec{E}$ are possible external fields (acting on a positively charged particle), and the spin axis is given by the purple arrow that rotates upward in a plane perpendicular to $\vec{E}$. If the initial condition begins with the spin parallel to the velocity, then the rotation caused by the EDM will change the vertical component of the beam polarization. This becomes the signal observed by a polarimeter located in the ring. This device allows beam particles to scatter from nuclei in a fixed bulk material target (black). The difference in the scattering rate between the left and right directions (into the polarimeter) is sensitive to the vertical polarization component of the beam. Continuous monitoring will show a change in the relative left-right rate difference during the time of the beam storage if a measurable EDM is present [4].

2.2.2 Concept of Frozen Spin

The angular frequencies ($\vec{\Omega}$) in Eq.(2.2) are defined with respect to the momentum vector of the particle which itself is changing as the particle travels around its orbit. Because the magnetic moments of all particles carry an anomalous part, the polarization will in general rotate in the plane of the storage ring relative to the beam path. This rotation must be suppressed by making $\vec{\Omega}_{MDM} = 0$, a condition called "frozen spin"[4].

In a magnetic ring, this condition requires that (since $\vec{\beta}.\vec{B} = 0$) in Eq.(2.3) (for only electric field plates in a ring with radial electric field shown in Eq.(2.6) to bend particles in a closed orbit). As $\vec{B} = 0$ in all electric rings the third term of Eq.(2.4) which is $\beta \times \vec{B}$, cancels, if

$$\gamma = \sqrt{1 + \frac{1}{G}} \tag{2.5}$$

For the proton with $G = 1.79285$ yields $\gamma = 1.2481$ and $p = 0.7007\,\mathrm{GeV/c}$. The kinetic energy of $T = 232.8\,\mathrm{MeV}$ fortunately comes at a point where the spin sensitivity of the polarimeter is near its maximum, creating an advantageous experimental situation.

For the deutron with $G < 0$, there is no solution for an all-electric ring, therefore magnetic fields must be included and the first and third terms of Eq.(2.3) cancel, if

$$E_r = \frac{GBc\beta\gamma^2}{1 - G\beta^2\gamma^2}. \tag{2.6}$$

In this situation, there is no need to constraint beam energy because Eq.(2.5) is not valid anymore for all particles with negative G. The electric field for deutron case must be pointing away from the center of the ring, thus reducing the bending of the beam from magnetic fields alone.

2.2.3 Systematical and Statistical Effects

The statistical error for one single machine cycle is given in [13]

$$\sigma_{stat} \approx \frac{2\hbar}{\sqrt{Nf}\tau PAE}. \tag{2.7}$$

Considering the parameters given in Table 2.1, the statistical error for one year of running (*i.e.*, 10000 cycles of 1000 s length) is

$$\sigma_{stat}(1year) = 2.4 \times 10^{-29}\,\mathrm{e\,cm} \tag{2.8}$$

The challenge is to suppress the systematic error to the same level. One idea is to have

Beam intensity	$N = 4.10^{10}$ per fill
Polarization	$P = 0.8$
Spin coherence time	$\tau = 1000\,\mathrm{s}$
Electric fields	E=8 MV/m
Polarimeter analyzing power	$A = 0.6$
Polarimeter efficiency	$f = 0.005$

Table 2.1: Parameters of the proton experiment

two simultaneous counter rotating beams in the ring which would reduce a large fraction of systematic errors because remanent radial magnetic fields effects will cancel each other. One beam is the time-reversal of other beam and the difference will show only the time-odd effects such as the EDM. For an all-electric proton ring, it's possible to implement this idea which would be advantageous to suppress many systematic errors (*i.e.*, geometric phases and remanent radial magnetic fields). Figure 2.3 shows two characteristics of an all electric storage ring experiment, the clockwise(CW) and counter-clockwise (CCW) beams and the opposite direction of polarization (parallel or anti-parallel) in separate beam bunches, which is important for geometric error cancellation in the polarimeter.

The proposed experiment of the EDM measurement is very sensitive to any phenomena which could effect the vertical component of the spin. Such systematic effects may be caused by unwanted electric fields due to imperfections of the focusing structure (such as misalignment of the components) or by magnetic fields penetrating the magnetic shielding or produced inside the shield by the beam itself, the RF cavity or gravity. A combination of several such phenomena, or combination of average horizontal spin and one of these phenomena, may as well lead to such systematic effects[4].

In many cases, as for example effects due to gravity, the resulting rotations of the spin into the vertical plane do not mimic an EDM because the observations for the two counter-rotating are not compatible with a time-odd effect. In this case, the contributions from the two counter-rotating beams tend to cancel, provided the forward and reverse polarimeters can be calibrated with sufficient precision. In some cases, as for example magnetic fields from the RF cavity, the resulting spin rotations into the vertical plane can be large.

One of the most dominating systematic effects is an average static radial magnetic field that mimics an EDM signal. For a 500 m circumference frozen-spin EDM ring, an average magnetic field of about 10^{-17} T produces the same vertical spin precession as the final experiment aims to identify for EDM of 10^{-29} e cm. To reduce the residual fields upto a nT level, a state-of-the-art magnetic shielding will be installed in the proposed ring. The vertical radial field will be measured with special pick-ups that must be installed at very regular locations along the beam pipe to measure the varying radial magnetic field component created by the bunched beam separation[4].

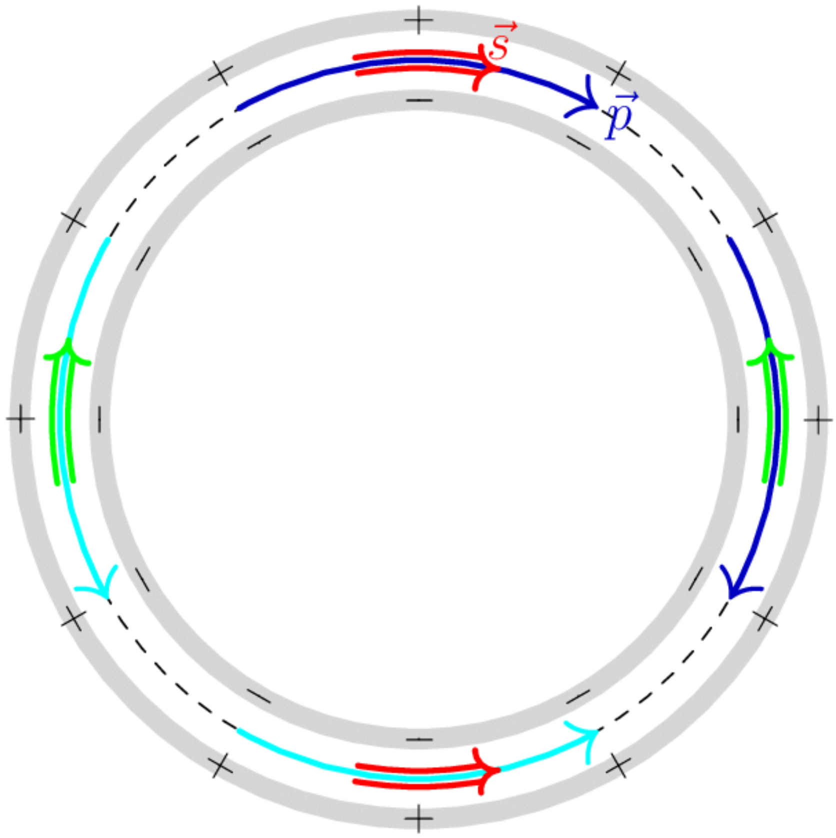

Figure 2.3: All electric storage ring with counter rotating beams (dark and light blue arrows), each with two spin projection states in the direction of momentum states (green and red arrows for each beam) [13]

2.2.4 Project Outline

The proton EDM experiment would be the largest electrostatic ring ever built with an exclusive feature like counter-rotating beams, demanding alignment and stability requirements. This ring may also require stochastic cooling and weak magnetic focusing depending on dual beam operation at a time. A strategy will be necessary to verify the EDM signal produced by the experiment after systematic errors substraction by a series of critical tests and independent analyses. After intensive discussions within the CPEDM[2], a plan for the final ring is decided which will proceed in three stages [4].

1. **Precursor Experiment** which is currently ongoing at COSY (COoler SYnchrotron at the Forschungszentrum Jülich) for the measurement of the deutron EDM.

2. **Proton Prototype Storage Ring** which would be first used to measure the proton EDM and to study the principles and effects for the final ring. (Detailed discussion is in the next chapters)

3. **All-electric Ring** which would be the final ring to measure the proton EDM with very high precision (sensitivity goal is 10^{-29} e cm)

[2] Charged Particle Electric Dipole Moment collaboration at Forschungszentrum Jülich

The aim of these stages is to get rid of systematic errors and gain very high precision in the EDM measurements by the implementation of new and unique techniques.

The project CPEDM is in a position to start with, since a conventional (*i.e.*, using magnetic deflection) storage-ring facility exists that provides all the required elements for R & D and will even allow a "proof-of-capability" measurement [4]. COSY, at the Institute for Nuclear Physics (IKP) FZJ Germany, is a storage ring for polarised proton and deuteron beams between 0.3(0.55)GeV/c and 3.7 GeV/c. Besides phase-space cooling (electron and stochastic cooling), well-established methods are used to provide, manipulate and investigate stored polarised beams.

By using deutrons with a momentum of 970 MeV/c at COSY with non-frozen spin, the polarization vector precession in the horizontal plane at 121 kHz relative to the velocity of beam which prevents a build-up of a vertical polarizaion due to the EDM. To allow for a build-up of the vertical polarization proportional to the EDM, a radio-frequency (RF) Wien-filter can be used [14]. It was installed in COSY in May 2017. In order to build-up vertical polarization, the Wein-filter has to be operated in resoanace with the spin precession frequency f_{spin}. The resonance condition is given by

$$f_{WF} = f_{rev}|k + v_s|, \quad k, \ integer, \tag{2.9}$$

where $v_s = f_{spin}/f_{rev}$ is the spin tune[3]. A build-up is only observable if the relative phase Φ between the fields of the Wien-filter and the horizontal polarization component match[4]. More details about precursor experiment can be obtained in [15].

The second stage is a proton prototype storage ring which will be focused in this thesis. The main goals are being discussed throughly in Chapter 3. Third and final stage would be the answer of many unattendable questions after acquiring very high precision in measuring the proton EDM. The summary of these stages is shown in Figure 2.4 below.

1 Precursor Experiment	2 Prototype Ring	3 All-electric Ring
dEDM proof-of-capability (orbit and polarization control; first dEDM measurement)	**pEDM proof-of-principle** (key technologies, first direct pEDM measurement)	**pEDM precision experiment** (sensitivity goal: 10^{-29} e cm)
- Magnetic storage ring - Polarized deuterons - d-Carbon polarimetry - Radiofrequency (RF) Wien-filter	- High-current all-electric ring - Simultaneous CW/CCW op. - Frozen spin control (with combined E/B-field ring) - Phase-space beam cooling	- Frozen spin all-electric (at p = 0.7 GeV/c) - Simultaneous CW/CCW op. - B-shielding, high E-fields - Design: cryogenic, hybrid,…
Ongoing at COSY (Jülich) 2014 → 2021	Ongoing within CPEDM 2017 → 2020 (CDR) → 2022 (TDR) Start construction > 2022	After construction and operation of prototype > 2027

Figure 2.4: Summary of the important features of the proposed stages[4]

[3] the number of spin revolutions per turn

CHAPTER 3

Motivation for Prototype EDM Storage Ring ("PTR")

As discussed in 2.2.4, the final stage of an all electric EDM ring will be constructed after implementing all unique techniques and ideas at the precursor experiment and the PTR. The consideration of these two earlier stages, is a necessity of time and budget because besides detailed studies of each and every possible aspect concerning the experiment, a real ground implementation always has its portion in terms of systematic and technical efforts. Starting from the available storage ring COSY which is a pure magnetic ring, a measurement of the deutron EDM after introducing deutron carbon polarimetry and a RF Wien-filter, is ongoing. However, implementing new techniques like counter-rotation of beams, deflection by pure electrostatic fields and studying all consequences of these techniques is not possible at COSY. Therefore, a small but a mock-up of the final EDM ring is considered, a proton PTR. Advantages of a prototype EDM ring are mentioned below [16]

- Storage of high intensity beams for sufficiently longer time (*i.e.* 1000 s).
- Injection of multiple polarization states (longitudinal and transverse) in clockwise (CW) and counter-clockwise (CCW) direction.
- Capability of the frozen spin method with simultaneously counter rotating beams.
- Introduction of magnetic shielding to minimize radial magnetic field components.
- Measurements of both CW and CCW polarized beams with a single target.
- Prevention of beam blow-up by electron cooling before injection or introducing stochastic cooling in the ring.
- Development and benchmarking of simulation tools.

Besides these goals, spin tracking calculations are also necessary to study the level of precision which is needed in the ring construction and the handling of systematic errors. For a detailed study of beam storage and the build-up of the EDM signal, one needs to track a large sample of particles over many turns. The PTR should be able to provide empirical experience needed to assess the systematic EDM errors.

3.1 Stages of PTR

Certainly, a PTR wouldn't be too big. It's circumference will be around 100 m with fourfold symmetry "squared" ring. To achieve all proposed goals from PTR, it has been divided into two modes.

1. All Electric Ring with $T = 30\,\mathrm{MeV}$
2. Electro-magnetic Ring with $T = 45\,\mathrm{MeV}$

The primary goal of mode 1 is to illustrate the performance routinely obtained in magnetic rings can be replicated in an all-electric ring and the goal of mode 2 is to implement the frozen spin concept with counter rotating beams. Detailed discussion about these two modes is below.

3.1.1 All Electric PTR Ring

The two *main* goals for the $T = 30\,\mathrm{MeV}$ all electric PTR mode can be figured out below

1. Show the capability of storing high intensity polarized proton beams.
2. Counter-rotate two high intensity polarized beams simultaneously to reduce systematic errors.

Technically, it would be sufficient for these goals to be achieved with unpolarized beams, since there is no reason to suppose that the storage capability depends in any way on the state of the beam polarization. The proton intensity goal has been set conservatively low to avoid distractions associated with preserving polarization through the injection process. This can be improved later, using well-understood experimental techniques.

Investigation of this mode of PTR can help to modify possibilities necessary to upgrade the second mode of PTR. Such as, use of stochastic cooling is also under consideration. Besides it, it is not sure, whether completely cryogenic vacuum will be necessary or not. The probability of a regenerative breakdown mechanism that could limit proton beam current, also depends on the type of vacuum. Such kind of breakdown could be initiated by a temporarily free electron, being accelerated toward the positive electrode. Secondary electrons created on impact, would be immediately re-captured, but photons produced could strike the other electrode, producing secondary electron emission that could lead to regenerative failure. No such phenomenon has ever been observed in magnetic rings, but this is irrelevant, since there is no corresponding electron acceleration present. Some proton intensity limitations in non-relativistic rings seem consistent with such interpretation. But no such limitation has been observed in electrostatic separators in either electron or proton high energy storage rings. Any such breakdown mechanism would apparently tend to be moderated by superimposed magnetic fields.[4]

The possibility of significant upgrading of positioning and alignment is also anticipated between stages 1 and 2. Ferrite kickers, assumed for stage 1, may need to be replaced by air core or electrostatic kickers for stage 2. Greatly improved critical analysis of beam position monitor (BPM) performance is also expected in stage 1, for possible inclusion in stage 2. Similar investigations of the stability of basic mechanical and electrical parameters will be performed.

3.1.2 Electro-magnetic PTR

The stage of $T = 45\,\mathrm{MeV}$ will focus on the development of operational capabilities and identification of the issues that are needed to be resolved before the final all electric ring can be built. Following goals are expected to gain from this stage of PTR

1. Experimental methods are needed to be developed and illusterated for measuring the proton EDM with superimposed electric and magnetic bending. Though the compact design of PTR will put limits on the precision of the EDM measurements but data needed for extrapolation to the full scale ring has to be obtained from the PTR.

2. Magnetic shielding is another uncertain issue. As magnetic field needs to be reversed periodically to suppress systematic deviations and this reversal should be done rapidly, therefore the magnet should be iron-free. One of the unique ideas for this fielding is shown in Figure. 3.1 with copper instead of iron and it would improve shielding by at least one or two orders of magnitude. But it requires detailed understanding of the apparatus, that can be studied by simulation and later experimentally. Certainly magnetic shielding could be upgraded in the interval between stages. No active field control based on magnetic measurements is planned for stage 1, but could, optionally, be developed for stage 2.

3. The fundamental physical significance of gravitational effects on the EDM measurement is debatable and needs an experimental ground to observe if there would be any fake EDM due to general relativity [4].

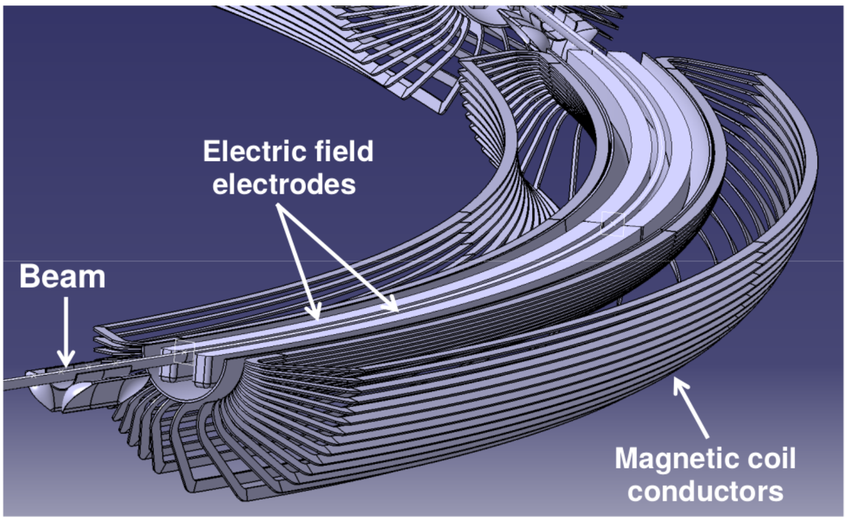

Figure 3.1: A special design of magnetic shielding over electric bending elements with copper bars to overlap electric and magnetic fields to avoid fringe field effect [4].

3.1.3 Basic Parameters of PTR

The squared fourfold structure of the PTR has been finalized with 8 m long straight sections. The basic layout of the PTR is shown in Figure 3.2. It consists of 4 unit cells each of them has bending of 90°. Each cell contains a focusing structure F-B-D-B-F, where F is a focusing quadrupole, D is a defocusing quadrupole, and B is an electric/magnetic bending unit. The straight sections have to house separate injection regions for clockwise (CW) and counter-clockwise (CCW) beam operation. There will also be straight section quadrupole (QSS) in the centre of each of the straight section, to provide additional tuning possibilities.

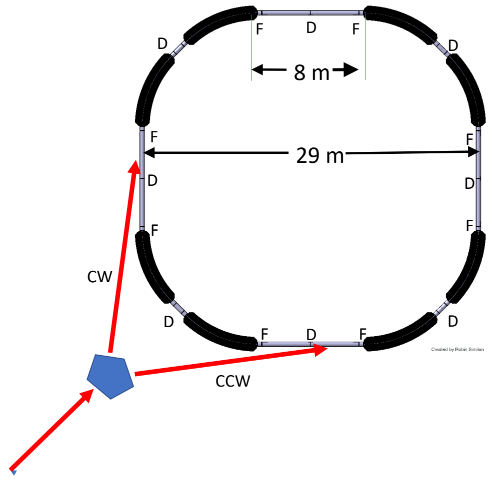

Figure 3.2: The basic layout of the PTR, consisting of eight electrodes, three families of quadrupoles (focusing:QF, defocusing :QD and straight section: QSS) with total circumference of around 100 m [16].

The basic beam parameters[1] of PTR [4] for both stages which are discussed above, are given in Table 3.1 and Table 3.2 shows the numbering of elements and geometery defined for PTR design[4].

3.1.4 Tune Variability

The quadrupoles in the straight sections of the ring as shown in Fig 3.2, are helpful to get more variability in betatron tunes to smoothen the optical functions (discussed below) to further reduce systematic errors and enhance beam lifetime (discussed below). The tuning capability is useful to adjust the ring for

1. strong focusing with larger beam acceptance and longer beam lifetime but with more systematic errors as radial magnetic fields become more dominant.

2. ultra weak focusing when radial magnetic fields are negligible so, systematic errors would be at its minimum but unfortunately beam lifetime reduces too.

[1] For curverlinear coordinate system (x,y,s), with x,y for horizontal and vertical motion respectivel and s for longitudinal direction

Parameter	E only	ExB	unit
Kinetic Energy (T)	30	45	MeV
$\beta = v/c$	0.247	0.299	
Momentum (pc)	239	294	MeV
Magnetic rigidity $B\rho$	0.798	0.981	T m
Electric rigidity	59.071	87.941	MV
γ (Lorentz factor)	1.032	1.048	
Emittance ($\epsilon_x = \epsilon_y$)	1.0	1.0	mm mrad
Acceptance ($a_x = a_y$)	1.0	1.0	mm mrad

Table 3.1: Basic beam parameters

		unit
No. of B-E deflectors	8	
No. of arc D quads	4	
No. of arc F quads	8	
quad length	0.400	m
straight length	0.800	m
bending radius	8.861	m
electric plate length	6.959	m
arc length (45°)	15.7	m
total circumference	102.39	m

Table 3.2: Ring elements and geometry parameters

Therefore, to find an optimized lattice which balances both aspects that reduces systematic effects significantly and improves beam lifetime as well, is one of the challenges for the PTR. The lattice's tune flexibilty can be observed by changing the quadrupole strengths. This is investigated in chapter 5 section 5.3.2 of this thesis.

CHAPTER 4

Linear Beam Dynamics

The knowledge of beam dynamics is important to study beam simulation of any storage ring. Therefore this chapter gives a breif introduction of beam dynamics in a periodic closed lattice and introduces the notation used in this thesis.

4.1 Fundamentals of Charged Particle Beam Optics

The force which bends and directs the charged particles beam or provides focusing to hold particles close to the ideal path is known as the Lorentz force and is derived from the electric and magnetic fields through the Lorentz equation.

$$\vec{F}_L = q(\vec{E} + \vec{v} \times \vec{B}) \tag{4.1}$$

where q is electric charge and $\vec{E}$ and $\vec{B}$ are the electrical and magnetic field vectors recpectively and $\vec{v}$ is the velocity of the particle. The evolution of particle trajectories under the influence of the Lorentz forces is called **beam dynamics** or **beam optics**. For relativistic particles with a momentum perpendicular to magnetic field, electric and magnetic fields have the same impact on the particles if $\vec{E} = c\vec{B}$ is fulfilled.

4.1.1 Coordinate System

A beam consists of many particles and each of those particles contributes to the propagation of the beam through the elements of the ring. The main purpose of investigating beam dynamics is to determine deviations from a specified reference orbit for all particles in the beam. Since describing these deviations with respect to a static laboratory coordinate system in most cases turns out to be cumbersome, it is convenient to choose a co-moving cartesian coordinate system[17]. Its origin follows the reference particle which moves along the reference orbit with momentum $\vec{p}_0$. The reference orbit, also called closed orbit, is defined by the field distribution in the accelerator and is the one-turn periodic path of the reference particle. It can be measured as the averaged beam position at every element over a time much larger than the revolution time. The current position of the coordinate system on the reference orbit is called s and is calculated from an arbitrary but fixed starting point [18]. Figure 4.1 shows the idea of such a coordinate system.

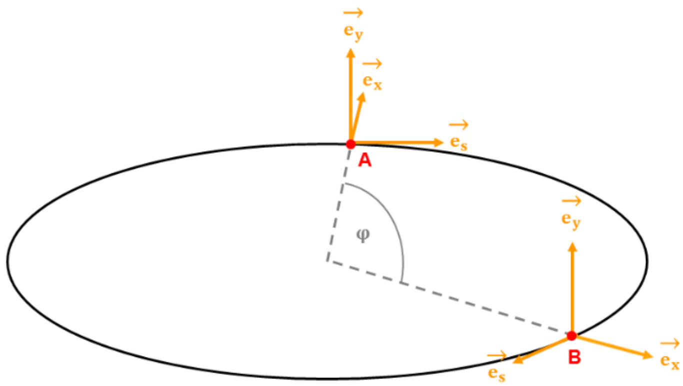

Figure 4.1: Co-moving coordinate system with its origin located at the reference particles' position. The s-axis is tangential to the reference orbit, the x-axis points in radial direction and y denotes the vertical direction [19].

The unit vector $\vec{e_s}$ always points along the reference particles momentum, while the unit vectors $\vec{e}_x$ and $\vec{e}_y$ span the plane orthogonal to $\vec{e}_s$, where $\vec{e}_x$ lies collinear and $\vec{e}_y$ is perpendicular to the plane of the storage ring. Assuming the reference path always lies in the horizontal plane, the transformation of the coordinate system from point A to point B on the reference path is given by

$$\vec{e}_{x,B} = \vec{e}_{x,A}\cos(\varphi) + \vec{e}_{s,A}\sin(\varphi) \tag{4.2}$$
$$\vec{e}_{y,B} = \vec{e}_{y,A} \tag{4.3}$$
$$\vec{e}_{s,B} = -\vec{e}_{x,A}\sin(\varphi) + \vec{e}_{s,A}\cos(\varphi) \tag{4.4}$$

where

$$\varphi = \int_A^B \frac{ds}{\rho(s)}, \tag{4.5}$$

with bending radius $\rho(s)$[20].

The change of the unit vectors over time is given by

$$\dot{\vec{e}_x} = \frac{d\vec{e}_x}{d\varphi}\frac{d\varphi}{dt} = \frac{1}{\rho}\dot{s}\vec{e}_s, \tag{4.6}$$
$$\dot{\vec{e}_y} = 0, \tag{4.7}$$
$$\dot{\vec{e}_s} = \frac{d\vec{e}_s}{d\varphi}\frac{d\varphi}{dt} = -\frac{1}{\rho}\dot{s}\vec{e}_x \tag{4.8}$$

To describe the trajectory of a particle $r(\vec{s})$ in the beam it is thus sufficient to know its position with respect to the trajectory of the reference particle $r_0(\vec{s})$. Using the transverse deviations from the reference orbit of a single particle $x(s)$ and $y(s)$, its trajectory can be parametrized as [18]

$$\vec{r}(s) = \vec{r}_0(s) + x(s)\vec{e}_x(s) + y(s)\vec{e}_y(s) \tag{4.9}$$

4.1.2 Equation of Motion

The equations of motion are derived for particles under the influenece of electromagnetic fields. Eq.(4.9) describes the general trajectory of a particle relative to the reference orbit. To formulate the equations of motion, the time derivatives of $r(s)$ are needed. By using Eq.(4.6) to Eq.(4.8)

$$\dot{\vec{r}}(s) = \dot{x}\vec{e}_x + \dot{y}\vec{e}_y + \left(1 + \frac{x}{\rho}\right)\dot{s}\vec{e}_s \tag{4.10}$$

$$\ddot{\vec{r}}(s) = \left[\ddot{x} - \left(1 + \frac{x}{\rho}\right)\frac{\dot{s}^2}{\rho}\right]\vec{e}_x + \ddot{y}\vec{e}_y + \left[\frac{2}{\rho}\dot{x}\dot{s} + \left(1 + \frac{x}{\rho}\right)\ddot{s}\right]\vec{e}_s. \tag{4.11}$$

At every point in time the position s on the path through the accelerator is uniquely determined and can therefore be used as the independent variable.

Hence time derivatives can be transformed into derivatives with respect to s resulting in [20]

$$\dot{\vec{r}}(s) = x'\dot{s}\vec{e}_x + y'\dot{s}\vec{e}_y + \left(1 + \frac{x}{\rho}\right)\dot{s}\vec{e}_s, \tag{4.12}$$

$$\ddot{\vec{r}}(s) = \left[x''\dot{s}^2 + x'\ddot{s} - \left(1 + \frac{x}{\rho}\right)\frac{\dot{s}^2}{\rho}\right]\vec{e}_x + (y''\dot{s}^2 + y'\ddot{s})\vec{e}_y + \left[\frac{2}{\rho}x'\dot{s}^2 + \left(1 + \frac{x}{\rho}\right)\ddot{s}\right]\vec{e}_s. \tag{4.13}$$

The Lorentz force acts on particles traversing electromagnetic fields. Assuming a pure magnetic accelerator it reduces to

$$m\ddot{\vec{r}}(s) = q(\dot{\vec{r}}(s) \times \vec{B}). \tag{4.14}$$

Assuming a pure magnetic storage ring consisting only of dipoles and quadrupoles with only vertical magnetic fields the equations of motion for a particle traversing the magnetic structure are given by [17]

$$x''(s) + \left(\frac{1}{\rho^2(s)} - k(s)\right)x(s) = \frac{1}{\rho(s)}\frac{\Delta p}{p_0} \tag{4.15}$$

$$y''(s) + k(s)y(s) = 0 \tag{4.16}$$

These equations form the basis of calculations in the linear beam optics.

4.1.3 Transverse motion

By ignoring the dispersive effecrs, i.e $\Delta p/p_0 = 0$, the Eq.(4.15) and Eq.(4.16) become second order homogeneous differential equations of the form

$$x''(s) = K(s)x(s) = 0, \tag{4.17}$$

$$y''(s) = k(s)y(s) = 0, \tag{4.18}$$

with

$$K(s) = \frac{1}{\rho^2(s)} - k(s). \tag{4.19}$$

Eq.(4.17) and Eq.(4.18) are known as **Hill's differential equations.**

Since both equations are of equal form and thus can be solved with the same procedure, the following calculations will only consider the solution in horizontal direction. The vertical solution can be found analogously. Except for the s dependent coefficient K(s) which is periodic over one turn with a length of C, i.e. K(s+C) = K(s), the differential equation resembles the one of a harmonic oscillator. For simplicity the s dependence will not be explicitly mentioned in every step in the following calculations. By analogy with the harmonic oscillator the ansatz

$$x(s) = Au(s)\cos[\Psi(s) + \Psi_0] \tag{4.20}$$

is chosen, where A and Ψ_0 are the constants of integration defining the trajectory of every individual particle. Inserting Eq.(4.20) into Eq.(4.17) leads to

$$\underbrace{(u'' - u\Psi'^2 + uK)}_{\mathrm{I}}\cos(\Psi + \Psi_0) - \underbrace{(2u'\Psi' + u\Psi'')}_{\mathrm{II}}\sin(\Psi + \Psi_0) = 0. \tag{4.21}$$

Independently of each other, terms I and II must vanish for Eq.(4.21) to hold.Thus

$$u'' - u\Psi'^2 + uK = 0 \tag{4.22}$$

and

$$2u'\Psi' + u\Psi'' = 0. \tag{4.23}$$

integarting Eq. (4.23) twice yields

$$\Psi'(s) = \frac{1}{u^2} \tag{4.24}$$

and

$$\Psi(s) = \int_0^s \frac{ds'}{u^2(s')}. \tag{4.25}$$

Inserting Eq.(4.24) into Eq.(4.22) the differential equation of $u(s)$ can finally be written

$$u''(s) + K(s)u(s) = \frac{1}{u^3(s)}, \tag{4.26}$$

which has a uniquely defined periodic solution $u(s)$. Introducing the betatron function $\beta(s)$ with

$$\beta(s) = u^2(s) \tag{4.27}$$

the general solution of Hill's differential equation are pseudo-harmonic oscillations, so called betatron oscillations, about the reference orbit with a s dependent amplitude given by

$$x(s) = A\sqrt{\beta(s)}\cos[\Psi(s) + \Psi_0] \tag{4.28}$$

and

$$x'(s) = \frac{A}{\sqrt{\beta(s)}}\left[-\alpha(s)\cos[\Psi(s) + \Psi_0] - \sin[\Psi(s) + \Psi_0]\right]. \tag{4.29}$$

where

$$\alpha(s) := \frac{\beta(s)}{2} \quad \text{and} \quad \gamma(s) := \frac{1+\alpha^2(s)}{\beta(s)}. \tag{4.30}$$

The parameter A denotes the amplitude of the oscillation and Ψ_0 indicates the initial phase. The functions $\alpha(s), \beta(s)$ and $\gamma(s)$ are known as the **optical functions** or **Twiss parameters**. The **betatron tune** (Q), defined as the number of betatron oscillations per turn, is calculated by[18]

$$Q = \frac{1}{2\pi}\int_s^{s+C} \Psi' ds = \frac{1}{2\pi}\int_s^{s+C} \frac{ds'}{\beta(s)}. \tag{4.31}$$

The particles thus perform oscillations about the reference orbit. The oscillation amplitude is dependent on the magnetic structure $\beta(s)$ and on the integration constant A. It is different for each particle as A is an intrinsic quantity of a particle. Figure 4.2 illustrates the transverse motion of several particles along the accelerator. The particle with the largest value of A defines the envelope of the particle trajectories. All other particles move within the boundaries defined by this envelope.

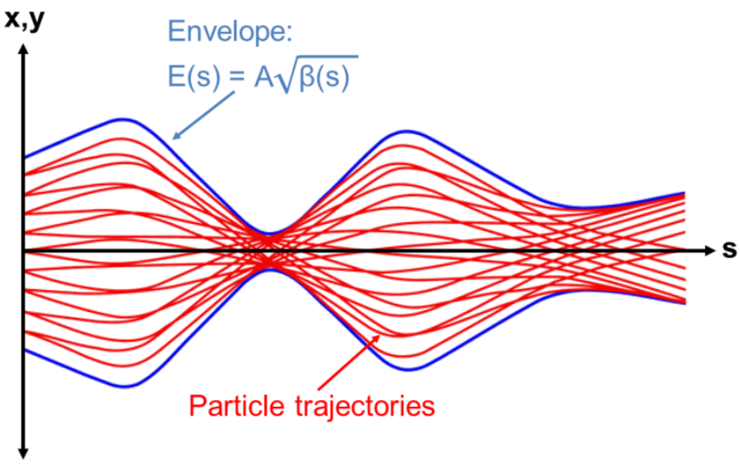

Figure 4.2: The transverse motion of all particles in the beam is limited by the particle with the largest value of A. Its trajectory along the ring forms the envelope for all other particles. [20].

4.1.4 Dispersion

Considering now particles with a non-vanishing momentum deviation $\Delta p/p_0$. From Eq.(4.17) it follows that a momentum deviation only influences the trajectory of the particle in sections with a finite bending radius ρ. It is therefore sufficient to solve the equation of motion only within a bending magnet with constant bending radius ρ where a vanishing quadrupole contribution, i.e. a homogeneous dipole field is assumed. Eq.(4.17) then turns into

$$x''(s) + \frac{1}{\rho^2}x(s) = \frac{1}{\rho}\frac{\Delta p}{p_0}. \tag{4.32}$$

The dispersion function D(s) is defined for a momentum spread of $\Delta p/p_0 = 1$ and fulfills the differential equation

$$D''(s) + \frac{1}{\rho^2}D(s) = \frac{1}{\rho}, \tag{4.33}$$

with the periodicity conditions

$$D(s+C) = D(s), \tag{4.34}$$
$$D'(s+C) = D'(s) \tag{4.35}$$

and the boundary conditions

$$D(0) = D_0, \tag{4.36}$$
$$D'(0) = D_0'. \tag{4.37}$$

The modified horizontal motion of a particle is then given by

$$x_{total}(s) = x(s) + x_D(s) = x(s) + D(s)\frac{\Delta p}{p_0} \tag{4.38}$$

where $x(s)$ describes the betatron oscillation and $x_D(s)$ represents the additional motion due to momentum deviation [18].

The differential equation Eq.(4.33) is solved using an ansatz of a harmonic oscillation and the particular solution [20]

$$D_p(s) = \rho$$

Incorporating the boundary conditions finally leads to

$$D(s) = D_0 \cos\left(\frac{s}{\rho}\right) + \rho D_0' \sin\left(\frac{s}{\rho}\right) + \rho\left(1 - \cos\left(\frac{s}{\rho}\right)\right) \tag{4.39}$$
$$D'(s) = -\frac{D_0}{\rho}\sin\left(\frac{s}{\rho}\right) + D_0'\cos\left(\frac{s}{\rho}\right) + \sin\left(\frac{s}{\rho}\right). \tag{4.40}$$

Besides the betatron oscillations the particles with non-vanishing momentum deviations now oscillate around a dispersion trajectory defined by $\Delta p/p_0$. The path length of a particle in the accelerator therefore differs from the reference orbit length. It can easily be shown that a dispersive particle travels the distance [20]

$$ds = \frac{\rho + x_D}{\rho}ds_0 \tag{4.41}$$

at positions with non-vanishing dispersion, where ds_0 denotes the path length the reference particle passes in the same time interval. With L_0 denoting the path length of the reference particle the total path length over one turn is given by

$$L = L_0 + \Delta L = \oint \frac{\rho + x_D}{\rho}ds = \oint ds + \frac{\Delta p}{p_0}\oint \frac{D(s)}{\rho(s)}ds \tag{4.42}$$

which leads to a change in the path length of

$$\Delta L = \frac{\Delta p}{p_0}\oint \frac{D(s)}{\rho(s)}ds. \tag{4.43}$$

4.1.5 Chromaticity

Particles with a momentum deviation from the reference momentum p_0 are exposed to a slightly different quadrupole strength than the reference particle and are therefore focused differently. The error of chromatic aberration is already well known from optics. The effect is illustrated in Figure 4.3 , where the focusing quadrupole is represented by a focusing lens.

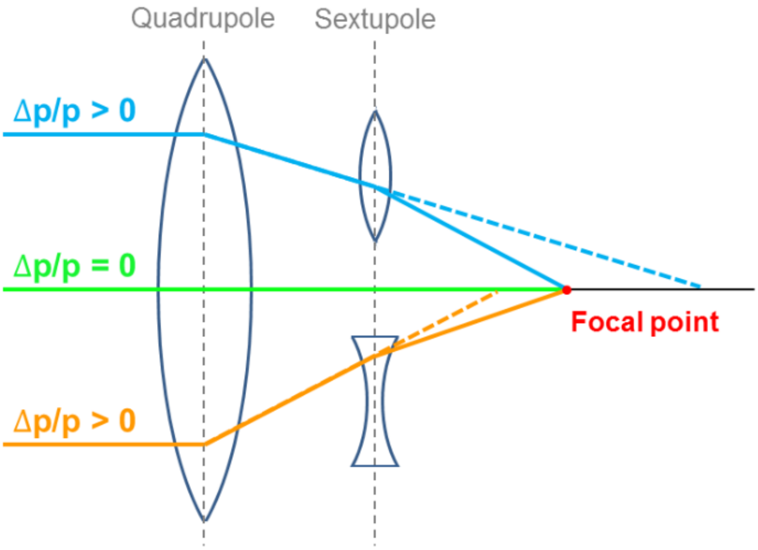

Figure 4.3: The effect of momentum dependence of the focusing strength of a quadrupole is called chromaticity. Depending on the radial position of the particles, sextupoles create quadrupole components which can correct the chromaticity effect if they are positioned in dispersive regions. [20].

Assuming only small deviations from the reference momentum the quadrupole strength seen by a particle with momentum $p = p_0 + \Delta p$ is given by

$$k(p) = -\frac{q}{p}g = -\frac{q}{p_0 + \Delta p}g \approx -\frac{q}{p_0}(1 - \frac{\Delta p}{p_0})g = k_0 - \Delta k. \tag{4.44}$$

A momentum deviation can be interpreted as a quadrupole error [20]

$$\Delta k = \frac{\Delta p}{p_0}k_0. \tag{4.45}$$

One can show that the quadrupole error leads to a change in the betatron tune over a distance ds of [20]

$$dQ = \frac{\Delta p}{p_0}\frac{1}{4\pi}k_0\beta(s)ds. \tag{4.46}$$

Since the particle retains its momentum deviation over many turns, all quadrupoles have the same error from the particles perspective. Hence the total tune shift is calculated by integrating over all quadrupoles in the accelerator. The dimensionless quantity

$$\xi := frac\Delta Q\frac{\Delta p}{p_0} = \frac{1}{4\pi}\oint k(s)\beta(s)ds \tag{4.47}$$

is called natural chromaticity and increases with growing focusing strength $k(s)$. The main contributions come from quadrupoles with large focusing strengths where the betatron function is large. Since a tune shift can lead to a working point at optical resonances [17] and hence to a loss of particles, chromaticity has to be compensated for. A correction is performed at positions where the particles are separated according to their momenta, i.e. at positions with non-vanishing dispersion. At these positions sextupole magnets are installed which have a focusing strength dependent on the transverse position. The principle of compensating chromaticity using sextupoles is schematically illustrated in Figure 4.3.

4.2 Transfer Matrices for Particle trajectories

The particle trajectory in an element can be expressed in terms of transfer matrices. These transfer matrices are solutions of Eq.4.17 and Eq.4.18. Considering the trajectory equation 4.17 for quadrupole element, (with its strength k and length l and no beam bending (1/R=0) in it) which is simplified as

$$x''(s) - kx(s) = 0 \qquad (k = \text{const}). \tag{4.48}$$

This homogeneous and linear second-order differential equation has the form of a normal oscillation equation which may be directly solved analytically. In the case of a horizontally **defocusing** magnet with $k > 0$, the solution can be given as

$$x(s) = A\cosh\sqrt{k}s + B\sinh\sqrt{k}s \tag{4.49}$$

$$x'(s) = \sqrt{k}A\sinh\sqrt{k}s + \sqrt{k}B\cosh\sqrt{k}s. \tag{4.50}$$

The constants of integration A and B are determined in the usual way by the initial conditions. Assuming that at the start of the magnet $s = 0$ the particle trajectory has the displacement x_0 and gradient x'_0 relative to the orbit. At this point the trajectory is thus defined by the trajectory vector

$$X_0 = \begin{pmatrix} x_0 \\ x'_0 \end{pmatrix} = \begin{pmatrix} x(0) \\ x'(0) \end{pmatrix} \tag{4.51}$$

Inserting these initial conditions into the solution Eq.(4.49) immediately gives

$$x(s) = x_0\cosh\sqrt{k}s + \frac{x'_0}{\sqrt{k}}\sinh\sqrt{k}s \tag{4.52}$$

$$x'(0) = x_0\sqrt{k}\sinh\sqrt{k}s + x'_0\cosh\sqrt{k}s \tag{4.53}$$

These equations, which describe the evolution of the trajectory vector from the start of a magnet to a point s within the magnet, may also be more elegantly written in matrix notation:

$$\begin{pmatrix} x(s) \\ x'(s) \end{pmatrix} = \begin{pmatrix} \cosh\sqrt{k}s & \frac{1}{\sqrt{k}}\sinh\sqrt{k}s \\ \sqrt{k}\sinh\sqrt{k}s & \cosh\sqrt{k}s \end{pmatrix} = \begin{pmatrix} x_0 \\ x'_0 \end{pmatrix} \tag{4.54}$$

Eq.(4.48) may be solved in the same way for a horizontally**focusing** quadrupole with $k < 0$ and for a zero-field drift region with $k = 0$. Depending on the choice of k following matrices are obtained

$$M = \begin{cases} \begin{pmatrix} \cos\sqrt{|k|}s & \frac{1}{\sqrt{|k|}}\sin\sqrt{|k|}s \\ -\sqrt{|k|}\sin\sqrt{|k|}s & \cos\sqrt{|k|}s \end{pmatrix} & \text{if } k < 0 \text{ (focusing)} \\ \\ \begin{pmatrix} 1 & s \\ 0 & 1 \end{pmatrix} & \text{if } k = 0 \text{ (drift section)} \\ \\ \begin{pmatrix} \cosh\sqrt{k}s & \frac{1}{\sqrt{k}}\sinh\sqrt{k}s \\ \sqrt{k}\sinh\sqrt{k}s & \cosh\sqrt{k}s \end{pmatrix} & \text{if } k < 0 \text{ (defocusing)} \end{cases} \tag{4.55}$$

Calculating the determinant of these matrices yields

$$\det \mathbf{M} = 1 \tag{4.56}$$

in every case, and the same is true in general for all transfer matrices in linear beam optics.

In the similar way, vertical motion of particles can be written in tranfer matrices and in most of the accelerator design codes, these transfer matrices are built-in.

The proposed ring would be one of the unique rings in its structure, because it will be built-up with all electric elements including quadrupoles and dipoles. But, all conventional storage rings usually contain magnetic elements, therefore, all tools of simulation in accelerator physics, till to-date consider magnetic fields for quadrupoles and dipoles. Though, manual addition of any type of element is always an option in advanced simulation softwares of accelerator physics. MAD-X [2] also has this feature to include elements by introducing their transfer matrices. The transfer matrices given in Eq.(4.55) are considered for magnetic quadrupoles. In case of electric quadrupole, the reference particles don't feel any difference when pass through it, therefore the same tranfer matrices given in Eq.(4.55) can be used for electric quadrupole when considering only ideal case[21]. In case of bending elements, there is big difference even for reference particles because responsible fields are electric fields instead of magnetic fields. Therefore, in MAD-X there is no need to add transfer matrices instead of build-in quadrupole elements for a nominal beam.

Therefore, only transfer matrices for bending elements are added into MAD-X. Several approaches have been scrutinized to build tranfer matrix for electrostatic deflectors. The transfer matrix for an electrostatic deflector is build by studying the particle motion inside deflector through hamiltonian.

Hamiltonian for Elelctrostatic Deflectors

The particle motion inside an electrostatic deflector is different than in other elements of a storage ring. When a particle enters the deflector of the ring, kinetic energy of particle changes in the presence of potential energy, however particle reagains this kinetic energy after leaving the deflector[21]. The cylindrical shape of electrostatic deflectors are more preferable over other shapes because of technicality. Electrostatic deflectors behave as combined function with strong vertical focusing.

Wollnik [22] also discusses all electrostatic deflectors with all possible shapes. The transfer matrix for cylinderical electrostatic deflectors with energy and time as longitudinal coordinates instead of momentum and distance. This choice is because, when a particle enters the electrodes off-axis, receives a "kick" to get into the potential field. This kick changes momentum P but not energy E thus momentum $\Delta P/P$ does not remain conserved. Therefore, a better approach is to consider energy E as a third longitudinal generalized coordinate. However, the first approch is to go for the conventional third longitudinal coordinate which is momentum and relative momentum deviation which was practiced by Rick Bartmaan [23], he showed, how a hamiltonian with electrostatic fields can be used to develop equations of motion of particle and the tranfer matrices can be written. He considered electrodes with curvature in horizontal as well as in vertical direction, though radius would be different in both sides. He transformed the third coordinate from time and energy to momentum and a relative distance deviation with respect to the reference particle *i.e.*, from $(t, -\Delta E)$ to (τ, Δ) where $\tau \equiv s - \beta ct, \Delta = \frac{\Delta p}{p}$.

This section is taken from R. Baartman [23] paper and confirmed by calculating equations of motion from hamiltonian. In electrostatic fields, for an independent variable s, on a reference trajectory curving in the xs-plane with curvature $h(s) = \frac{1}{R(s)}$ where R(s) is paricle bending radius, the exact Hamiltonian H for electrostatic bending is written as

$$H = \Delta - (1 + hx)\sqrt{1 + 2(\Delta - V) + \beta^2(\Delta - V)^2 - P_x^2 - P_y^2} \tag{4.57}$$

where $\Delta = \frac{\Delta p}{p}$ and P_x, P_y are transverse momenta and V is the electric potential with the linear optics arising from the second order Hamiltonian terms, given as

$$V = hx - h(h + k)\frac{x^2}{2} + hk\frac{y^2}{2}, \tag{4.58}$$

where $h = 1/R_0$ and $k = 1/R_y$,curvature in the bending and non-bend direction respectively. For the reference particle at $x = 0$, the electric field due to the potential Eq.(4.58) is

$$\varepsilon = -\frac{\partial \Phi}{\partial x} = -\frac{\beta c p_0}{q}\frac{\partial V}{\partial x}\Big|_{x=0} = \frac{\beta^2}{R_0}\frac{E_0}{q}. \tag{4.59}$$

In the non-relativistic limit, the electric field is twice the beam kinetic energy divided by charge and bend radius: $q\varepsilon = mv^2/R_0$. The first order terms in the resulting Hamiltonian all cancel as they should, Otherwise, the reference orbit would not be an orbit, so when expanded to the second order it is

$$\tilde{H} = \frac{P_x^2}{2} + \frac{P_y^2}{2} + \frac{\Delta^2}{2\gamma^2} - \frac{2 - \beta^2}{R_0}x\Delta + \frac{\xi^2}{2R_0^2}x^2 + \frac{\eta^2}{2R_0^2}y^2 \tag{4.60}$$

where parameters ξ and η are introduced as they parameterize the x and y focusing strengths:

$$\xi^2 + \eta^2 = 2 - \beta^2, \; \eta^2 = k/h = R_0/R_y$$

. For non-relativistic and the cylinderical bending, ξ equals to $\sqrt{2}$ and η equals to zero.

Thus, for all shapes of electrostatic deflectors, the equations of motion are obtained from given Eq.(4.57) in transverse (x(s) , y(s)) as well as in longitudinal (τ) direction with independent parameter s, These differential equations are

$$x''(s) + \frac{\xi^2}{R_0^2}x(s) - \frac{\Delta(2-\beta^2)}{R_0} = 0 \tag{4.61}$$

$$y''(s) + \frac{\eta^2}{R_0^2}y(s) = 0 \tag{4.62}$$

$$\tau'(s) + \frac{(2-\beta^2)}{R_0}x(s) - \frac{\Delta}{\gamma^2} = 0 \tag{4.63}$$

These differential equations Eq.(4.61), Eq.(4.62) and Eq.(4.63) satisfy the following solutions along with their angles (a(s) , b(s)) of inclination

$$x(s) = x_0\cos(\xi\theta) + a_0\frac{R_0}{\xi}\sin(\xi\theta) + \Delta_0\frac{R_0(2-\beta^2)}{\xi^2}(1-\cos(\xi\theta)) \tag{4.64}$$

$$a(s) = -x_0\frac{\xi}{R_0}\sin(\xi\theta) + a_0\cos(\xi\theta) + \Delta_0\frac{(2-\beta^2)}{\xi}\sin(\xi\theta) \tag{4.65}$$

$$y(s) = y_0\cos(\eta\theta) + b_0\frac{R_0}{\eta}\sin(\eta\theta) \tag{4.66}$$

$$b(s) = -y_0\frac{\eta}{R_0}\sin(\eta\theta) + b_0\cos(\eta\theta) \tag{4.67}$$

$$\tau(s) = -x_0\frac{2-\beta^2}{\xi}\sin(\xi\theta) - a_0\frac{2-\beta^2}{\xi^2}R_0(1-\cos\xi\theta) + \tau_0 + \Delta_0R_0\theta[\frac{1}{\gamma^2} - (\frac{2-\beta^2}{\xi})^2(1-\frac{\sin\xi\theta}{\xi\theta})] \tag{4.68}$$

where, $x_0, a_0, y_0, b_0, \tau_0, \Delta_0$ are initial values of respective coordinates and their angles of inclination and $\theta = s/R_0$.

Hence, the final transfer matrix of electrostatic deflector in transverse and longitudinal direction is

$$\begin{bmatrix} \cos\xi\theta & \frac{R_0}{\xi}\sin\xi\theta & 0 & 0 & 0 & \frac{2-\beta^2}{\xi^2}R_0(1-\cos(\xi\theta)) \\ -\frac{\xi}{R_0}\sin\xi\theta & \cos\xi\theta & 0 & 0 & 0 & \frac{2-\beta^2}{\xi}\sin\xi\theta \\ 0 & 0 & \cos\eta\theta & \frac{R_0}{\eta}\sin\eta\theta & 0 & 0 \\ 0 & 0 & -\frac{\eta}{R_0}\sin\eta\theta & \cos\eta\theta & 0 & 0 \\ -\frac{2-\beta^2}{\xi}\sin\xi\theta & -\frac{2-\beta^2}{\xi^2}R_0 1-\cos\xi\theta & 0 & 0 & 1 & R_0\theta[\frac{1}{\gamma^2} - (\frac{2-\beta^2}{\xi})^2(1-\frac{\sin\xi\theta}{\xi\theta})] \\ 0 & 0 & 0 & 0 & 0 & 1 \end{bmatrix} \tag{4.69}$$

This matrix is used to simulate the PTR lattice design for the first mode of 30 MeV, however, for the second mode which would have a magnetic field shield over the electrostatic field, the hamiltonian can be reconsidered and then corresponding equations of motion.

4.3 Beam Losses

A huge variety of mechanisms can lead to beam losses in accelerators and storage rings. For examples, beam gas interactions, intra-beam scattering, the Touscheck effect, RF noise, collective effects, transition crossing, equipment failures and many more. Losses have an impact on performance, such as degradation of the beam quality, the lifetime may be reduced or the emittance may increase. Losses lead to radio-activation, which can have an impact on machine availability and maintainability. Particles are lost in the vacuum chamber if their transverse trajectory amplitudes are larger than the dimension of the vacuum chamber. Therefore, it is important to understand all mechanisms which can cause large particles amplitudes.[24]

Beam Lifetime

The concept of cross-section (σ) in particle physics or in atomic physics concerns the interaction of elementary particles, nuclei or atoms with each other. In a simple geometrical interpretation of the cross-section it can be thought of as the area within which a reaction will take place. Thus the units of a cross-section are the units of an area, thus in nuclear physics, cross section is measured in units of barn where 1 barn = $10^{-24}\,\mathrm{cm}^2$.[25]

It is understandable to relate cross-section and the lifetime of a beam. It will be explained for a beam target interaction but it would be the same in particle with rest gas interactions as well.

Consider a beam of intensity I, crossing a target of thickness dx with a density of n atoms per cm^3 . This beam will now be attenuated by the collisions, and the change in intensity dI will be proportional to I, n and dx, shown in Figure 4.4.

$$dI = -\ln dx\sigma. \tag{4.70}$$

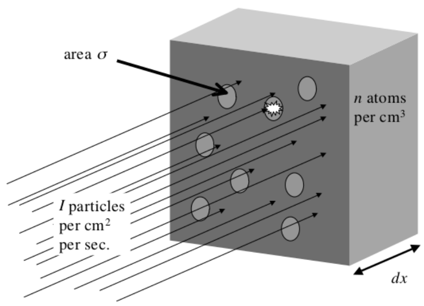

Figure 4.4: concept of cross section σ [25].

The target thickness traversed is given by $dx = vdt = \beta cdt$, where v and c are the velocities of the projectiles and the speed of light, respectively. The solution to Eq.(4.70) is then

$$I = I_0 e^{-\frac{t}{\tau}} \tag{4.71}$$

Hence the intensity will decay exponentially, with a lifetime τ by

$$\tau = \frac{1}{v\sigma n}. \tag{4.72}$$

When there are more processes of comparable significance, the cross sections should be added $\sigma_{total} = \sigma_1 + \sigma_2 + ..$, or the inverse lifetimes, the decay rates, should be added $1/\tau_{total} = 1/\tau_1 + 1/\tau_2 + ...$ in order to find the lifetime arising from all processes. This also applies to a real residual vacuum, where several atomic species are present.[24]

Thus, the cross-section which plays an important role in determining the beam lifetime, depends on many factors as well. It depends of course on the target particle, *i.e.*, the composition of the rest gas and also on the incident particles. In addition there is often a strong energy-dependence and a dependence on the type of interaction that is involved.

The interactions between charged particles and the target atoms can be classified as *elastic* and *inelastic* collisions. A collison is called *elastic* if the particles do not change identity during the interaction. It is possible to have elastic scattering both for the case of electromagnetic interaction and for the case of strong interaction. In the former case both particles must have a charge but in the latter case there is *elastic* scattering independent of the charge. All reactions that are not *elastic* are called *inelastic*. In this case there can be a change of nature of the particles and also new particles can be created[24].

The beam lifetime also depends on the final aperture available for the particle motion in the ring. Aperture limitation, does not necessarily mean a physical limitation, but also the limitation in the transverse plane due to the dynamic aperture, or the limitation in the longitudinal plan due to the RF-bucket size or the dynamic aperture for off-momentum particles (*i.e.*, particles with large synchrotron oscillation amplitudes)[26]. In the linear treatment of betatron oscillation the particle is lost, if its amplitude exceeds the aperture of the vacuum chamber. Usually, non-linear electromagnetic fields present in the ring cause a limitation of the maximum betatron amplitude, described by the dynamic aperture. Also in this case, the particle is lost at the physical aperture, but non linear effects blow up the betatron motion and limit the "stable" initial amplitudes to values far below the physical aperture[26].

Three main factors of beam losses are studied in this thesis in the presence of residual gas as well as target. In addition, interaction between beam of same particles known as "intra beam scatterings" also causes beam losses which will be discussed below.

4.3.1 Hadronic interaction

Accelerators mainly deal with protons, electrons, or ions. They are fundamentally very different particles. The size and mass are very different but also the compositeness and the forces with which they interact. There are four fundamental forces in nature. The forces of gravity and electromagnetism are familiar in everyday life. Two additional forces are introduced when discussing nuclear phenomena: the strong and weak interaction. The strong interaction is what holds the quarks together to form a proton while the weak force governs beta decay and neutrino interactions with nuclei. The forces which are relevant when considering beam gas interactions are the strong force and the electromagnetic force[24].

When two protons encounter each other, they experience both electromagnetic and strong forces simultaneously. However, the strong force dominates for head-on collisions and the electromagnetic forces dominate for peripheral collisions. Therefore, head-on collisions in case of beam-target or beam-gas interactions depend on the total cross section which can be obtained either by analytical formulas (shown below) suggested by the S-matrix and Regge theory or by experimental results[27]. The dependency of total *pp* interaction for the cross- section is on beam momentum or energy and can be calculateable as

$$\sigma_{tot} = a_1 + a_2 \left(\frac{s}{s_1}\right)^{a_3} \tag{4.73}$$

where s is the Mandelstam variable of the *pp* system, a_1, a_2 and a_3 are fit parameters and $s_1 = 1\,\mathrm{GeV}^2$ is a constant.

The beam loss rate is reciprocal to the beam lifetime and can be caculated by the following expression in analogy to Eq.(4.72)

$$\frac{1}{\tau_{loss}} = n_t \sigma_{tot} f_0 \tag{4.74}$$

where n_t is the target density, σ_{tot} is the total cross-section and f_0 is revolutional frequency of beam [28].

In case of residual gas, n_t is the number of scattering centers which under normal conditions at 0° and a gas pressure of 760 mm mercury and the number of scattering (n_t) centers in a homogeneous gas is equal to twice Avogadro's number Avo. For an arbitrary gas pressure P [17]

$$n_t = 2Avo \frac{P_{eq}(Torr)}{760}. \tag{4.75}$$

The factor 2 comes from the fact that homogeneous gases are composed of two atomic molecules, where each atom acts as a separate scattering center. This assumption would not be true for single atomic noble gases. P_{eq} is an equivalent pressure in *Torr* which is calculated from partial pressures of composite gasses.

In general, at high energies, the proton–nucleus cross-section has the same energy dependence as the proton–proton cross-section and as a rule of thumb the proton–nucleus cross-section can be deduced from the proton–proton cross-section according to [24]

$$\sigma_{pA} = \sigma_{pp} A^{0.7}$$

where A is the atomic mass number of residual gasses.

4.3.2 Coloumb Scatterings

Elastic scattering via the electromagnetic force is called Coulomb scattering and sometimes Rutherford scattering. Actually it was Rutherford who realized while observing results from scattering of alpha particles off a thin foil that the atom must have a very tiny nucleus compared to the size of the atom itself. The scattering angle depends on the impact parameter as illustrated in Fig.4.5. Small impact parameters give large scattering angles and vice versa[24].

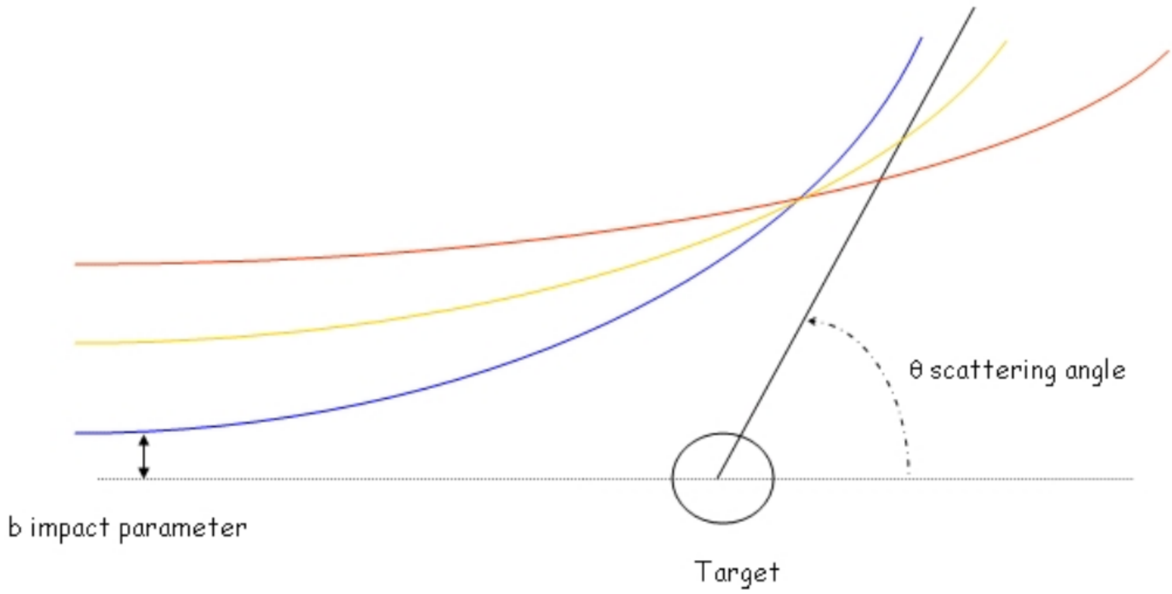

Figure 4.5: Relation between impact parameter and scattering angle [24].

The scattering process therefore is described by the classical Rutherford scattering with the differential cross section per atom

$$\frac{d\sigma}{d\Omega} = \frac{1}{4\pi\epsilon_0}\left(\frac{zZe^2}{2\beta cp}\right)^2 \frac{1}{\sin^4(\theta/2)} \tag{4.76}$$

where z is the charge multiplicity of the incident particle, eZ the charge of the heavy scattering nucleus, θ the scattering angle with respect to the incident path, Ω the solid angle with $d\Omega = \sin\theta d\theta d\phi$ and ϕ the polar angle[24]. Deviations from this very simple formula exist for small angles due to electronic screening effects of the atomic nucleus and for large angles due to the finite size of the nucleus as shown in Fig. 4.6

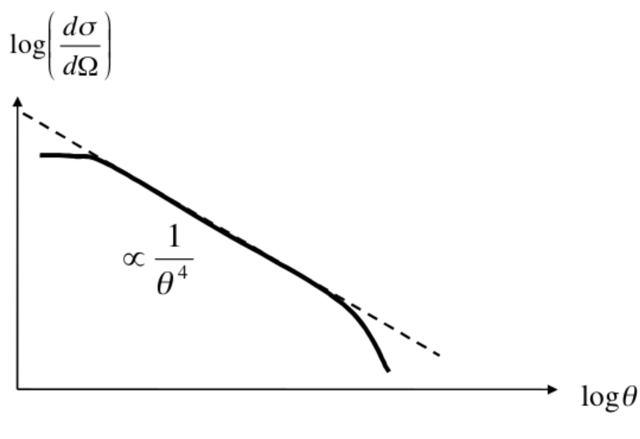

Figure 4.6: Qualitative behaviour of the Rutherford scattering cross section[25].

However, for the purpose of calculating the particle beam lifetimes due to elastic or Coulomb scattering screening effects by shell electrons and mathematical divergence problems at very small scattering angles are ignored.

The relevant cross section for calculation of lifetimes is the integral of this Rutherford cross section from θ_{acc}, the angle for which loss occurs, to a very large angle. This maximum angle doesn't need be specified since the most important contribution comes from the small angles. The resulting cross section is [17]

$$\sigma_{tot} = 2\pi \int_{\theta_{min}}^{\pi} \frac{d\sigma}{d\Omega} \sin\theta d\theta = \frac{4\pi Z_t^2 Z_i^2 r_p^2}{\beta_0^4 \gamma_0^2 \theta_{acc}^{*2}} \tag{4.77}$$

where Z_t and Z_i are the charge numbers of target and projectile and $r_p = 1.546 \times 10^{-18}\,\mathrm{m}$ is the classical proton radius. β_0 and γ_0 are the kinematical parameters of the circulating beam and θ_{acc} is the maximum scattering angle. The minimum aperture gives the maximum acceptable scattering angle and in the case of one small aperture A with a transverse betatron amplitude at this position of $\beta_\perp$, the angle is given by

$$\theta_{acc} = \sqrt{\frac{A}{\beta_\perp}}$$

where the betatron function $\beta_\perp$ is averaged over the whole circumference. In the case of a modern synchrotron radiation source, this aperture A would be the height of the undulator vacuum chamber with smallest gap. Hence, the beam loss rate for single Coloumb scattering is calculated by the same formula as given in Eq.(4.74). For beam-target interaction, the same equation is used after replacing σ_{tot} by the Rutherford scattering cross-section as given in Eq.(4.77).

However, in case of inhomogeneous residual gas, the beam loss rate can be calculated after substituting Eq.(4.77) and Eq.(4.75) in Eq.(4.74) and then replacing by

$$PZ_t^2 \rightarrow \sum_{i,j} P_i Z_j^2$$

where P_i is the partial pressure of the molecules i and Z_j the atomic number of the atom j in the molecule i.

Thus, the particle loss due to Coulomb scattering is most severe at low energies and increases with the acceptance of the beam transport line. Furthermore, the beam lifetime depends on the focusing in the transport line through the average value of the betatron function. If instead of averaging the betatron function, integrate the contributions to the beam lifetime along the transport line to find that the effect of the scattering event depends on the betatron function at the location of the collision and the probability that such a collision occurs at this location depends on the gas pressure there. Therefore, it is prudent to not only minimize the magnitude of the betatron functions alone but rather minimize the product β and pressure along the transport line. Specifically, where large values of the betatron function cannot be avoided, extra pumping capacity should be provided to reach locally a low vacuum pressure for long Coulomb scattering lifetime [17].

4.3.3 Energy Loss Straggling

Statistical fluctuations of the number and kind of collisions along the track of a particle cause the effect of "straggling" which means uneqaul energy loss along the tracks of particles that travel under identical conditions. Because of this effect, different particles that travel under same conditions have tracks of different lengths with different energies after transversing through target. In some cases, the average energy loss is not easily measurable, therefore, it is often more convenient to measure an energy loss distribution and from the distribution, the most probable loss or the median loss can be measured[29]. Much theoretical efforts have been spent to predict energy loss distributions. Depending on the target thickness one can differentiate between the single- plural- and multiple-scattering distributions, the Landau distribution [30], the Vavilov-distribution [31] and the Gaussian distribution.

The effective target thickness in a storage ring is considered to be small as compared to the circumference of ring. Therefore single-scattering distributions will be our concerned here. Thus, the energy loss distribution resulting from a single target traversal can be calculated using the elementary differential cross section $d\sigma/d\epsilon$. For beam-target concern about energy straggling, the evolution of the RMS[1] width of the energy loss distribution can be calculated without a detailed knowledge of the multiple scattering distributions. The corresponding mean-square energy deviation results from the accumulated contributions of single target traversals. Thus, for any distribution the mean-square energy deviation is just the mean-square value of the elementary single scattering distribution per target traversal multiplied by the number of turns[27].

In order to calculate the energy loss straggling one needs the differential cross section with respect to the energy loss. Neglecting the very small energy losses due to atomic excitations in the evaluation of the energy straggling and taking only the ionization processes into account the differential cross section can be written as [27]

$$\frac{d\sigma}{d\epsilon} = 2.55 \times 10^5 \,\mathrm{eV\,b}\frac{1}{\beta^2}\left(\frac{1}{\epsilon^2} - \beta^2\frac{1}{\epsilon\epsilon_{max}}\right) \text{ for } \epsilon_i \leq \epsilon \leq \epsilon_{max}, \tag{4.78}$$

$$\frac{d\sigma}{d\epsilon} = 0 \quad \text{for} \quad \epsilon < \epsilon_i \quad \text{and} \quad \epsilon_{max} < \epsilon.$$

Here, ϵ_i is the ionization energy (for hydrogen 13.6 eV) and ϵ_{max} is the maximum energy loss which occurs in a head-on collision with a target electron. Outside of the interval, where $\epsilon_i \leq \epsilon \leq \epsilon_{max}$ the differnetial cross-section $d\sigma/d\epsilon$ is zero. As an example, Fig.4.7 shows the differential cross section $d\sigma/d\epsilon$ as a function of the energy loss ϵ for antiprotons with a kinetic energy of 8.0 GeV. The unit of $d\sigma/d\epsilon$ is barn/eV.

[1]Root Mean Square

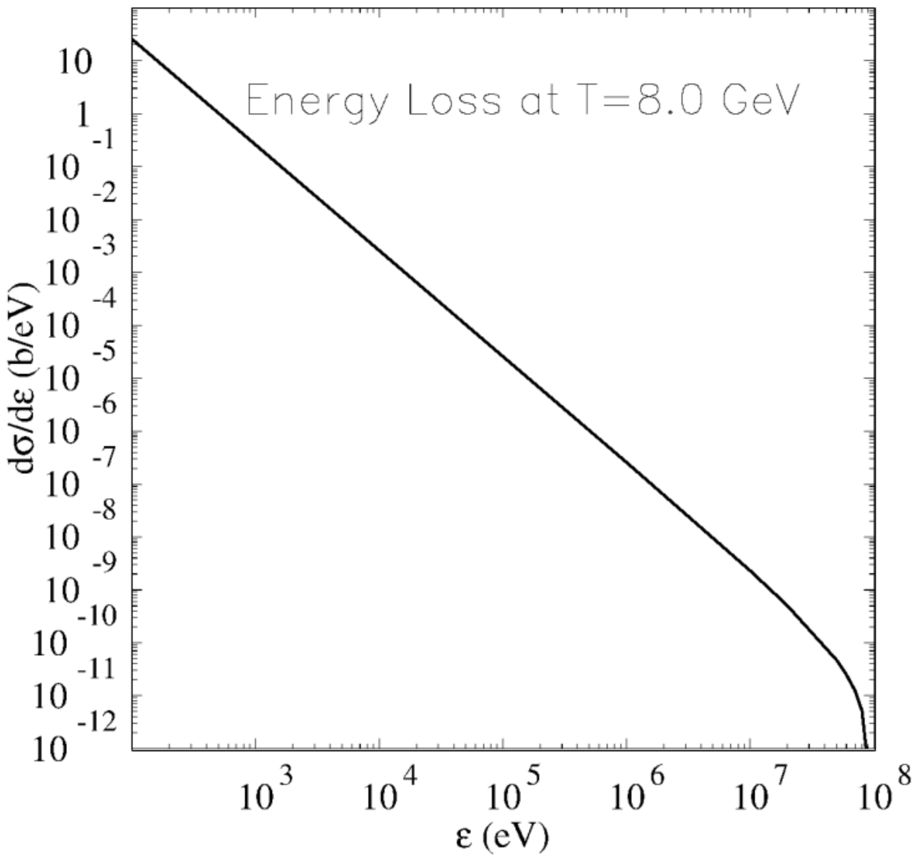

Figure 4.7: Differential cross section $d\sigma/d\epsilon$ vs. energy loss ϵ with 8 GeV kinetic energy of proton[27].

The energy loss straggling can be evaluated by calculating the second moment of the energy loss distribution [27],

$$\Delta\epsilon_{rms}^2 = N_t z_{eff} \int_0^{\epsilon_{max}} \epsilon^2 \left(\frac{d\sigma}{d\epsilon}\right) d\epsilon - \bar{\epsilon}^2. \tag{4.79}$$

Here, $N_t z_{eff}$ is the effective number of target atoms per cm^2. Neglecting the very small terms depending on ϵ_i and $\bar{\epsilon}$, one gets

$$\Delta\epsilon_{rms}^2 = \xi\epsilon_{max}\left(1 - \frac{\beta^2}{2}\right) \tag{4.80}$$

where ξ is a measure of the effective areal target density ρz_{eff},

$$\xi = 0.1535\frac{\mathrm{MeVcm}^2}{g}\frac{Z_1^2}{\beta}\frac{Z_2}{A_2}\rho z_{eff}. \tag{4.81}$$

The maximum energy loss can be calculated using the formula

$$\epsilon_{max} = \frac{2m_e c^2\beta^2\gamma^2}{1 + 2\gamma\frac{m_e}{M} + \frac{m_e^2}{M^2}}. \tag{4.82}$$

Here, β is the velocity and γ is the Lorentz factor of the beam, m_e the elctron mass and M the projectile mass. The corresponding maximum momentum deviation reads[27]

$$\delta_{max} = \frac{\gamma}{\gamma+1}\frac{\epsilon_{max}}{T} \tag{4.83}$$

where T is the beam kinetic energy. The resulting equaton for δ^2_{rms} is

$$\delta^2_{rms} = \left(\frac{\gamma}{\gamma+1}\right)^2 \frac{\Delta\epsilon^2_{rms}}{T^2}. \tag{4.84}$$

However, in an accelerator or storage ring, the maximum energy loss ϵ_{max} can possibly be too large for circulating beam energy and resulting momentum deviation can also become large. Therefore, the actual longitudinal momentum acceptance of a storage ring puts limitation on energy loss in the ring. Thus, energy loss due to beam-target or beam-gas interactions out of the longitudinal acceptance of the accelerator leads to beam losses. The probabilty for a loss per turn, P_{loss} can be calculated by integrating the differential cross section $d\sigma/d\epsilon$ from minimum energy due to limited longitudinal acceptance ϵ_{cut} to ϵ_{max} [27]

$$P_{loss} = Nx\int_{\epsilon_{cut}}^{\epsilon_{max}} \frac{d\sigma}{d\epsilon} d\epsilon = \xi \int_{\epsilon_{cut}}^{\epsilon_{max}} \left(\frac{1}{\epsilon^2} - \beta^2 \frac{1}{\epsilon\epsilon_{max}}\right) d\epsilon. \tag{4.85}$$

$$P_{loss} = \xi\left(\frac{1}{\epsilon_{cut}} - \frac{1}{\epsilon_{max}} - \frac{\beta^2}{\epsilon_{max}} \ln\frac{\epsilon_{max}}{\epsilon_{cut}}\right). \tag{4.86}$$

The corresponding longitudinal beam loss rate can be written

$$\frac{1}{\tau_{loss}} = P_{loss} f_0. \tag{4.87}$$

Longitudinal Limitation

In the longitudinal plane, the particle is lost either at the RF-acceptance limit or the momentum acceptance of the dynamic aperture. Similar to the transverse plane, the particles are oscillating in the longitudinal plane. The particles keep oscillating around the stable synchronous particle varying phase and dp/p, (see Fig. 4.8)[32].

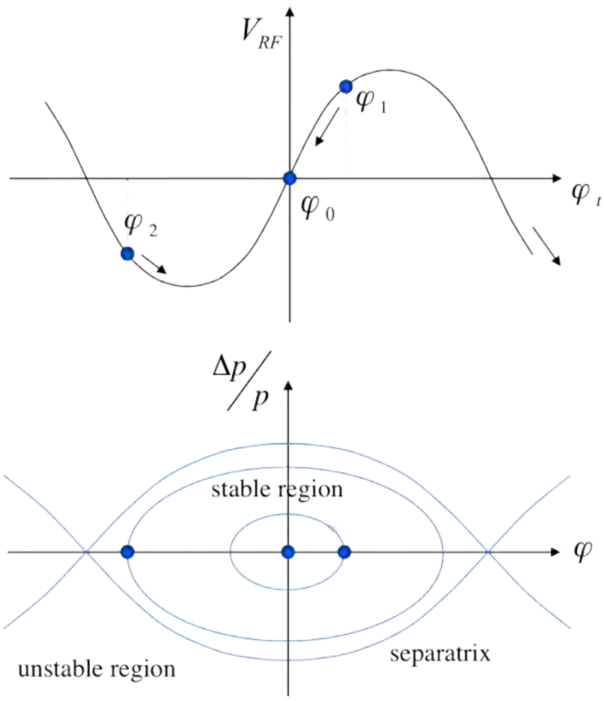

Figure 4.8: The longitudinal motion in the upper plot follows the trajectory in phase-space in the lower plot. The separatrix defines the limit of stable motion[32].

The **separatrix** defines the region of stable motion, the so-called bucket. The entire particle distribution needs to fit into the bucket to avoid particle losses. The bucket area, called the RF acceptance, is measured in electronvolts in the $\Delta E - \Delta t$ space, which is equivalent to $\Delta p/p - \Delta\phi$ space. The number of buckets around the ring corresponds to the harmonic number h. The bucket area is largest when the synchronous phase is 0°, or 180°, where the beam is not accelerated[32]. For acceleration, the synchronous phase has to move towards 90° and the buckets become smaller, as shown in Fig. 4.9. The RF acceptance increases with RF voltage, however, the RF acceptance plays an important role for losses created by RF capture and stored beam lifetime.

Since it found an invariant of motion, the equation for the separatrix by calculating at the phase $\phi = \pi - \phi_s$, where $\phi = 0$[32]

$$\frac{\dot{\phi}^2}{2} - \frac{\Omega_s^2}{\cos\phi_s}(\cos\phi + \phi\sin\phi_s) = -\frac{\Omega_s^2}{\cos\phi_s}(\cos(\pi-\phi_s) + (\pi-\phi_s)\sin\phi_s). \tag{4.88}$$

From this, we can calculate the second value ϕ_m where the separatrix crosses the horizontal axis, which is the other extreme phase for stable motion:

$$\cos\phi_m + \phi_m\sin\phi_s = \cos(\pi-\phi_s) + (\pi-\phi_s)\sin\phi_s. \tag{4.89}$$

It can be seen from the equation of motion that $\dot{\phi}$ reaches an extreme when $\ddot{\phi} = 0$, corresponding to $\phi = \phi_s$. Putting this value into Eq.(4.88) gives

$$\dot{\phi^2_{max}} = 2\Omega_s^2[2 + (2\phi_s - \pi)\tan\phi_s], \tag{4.90}$$

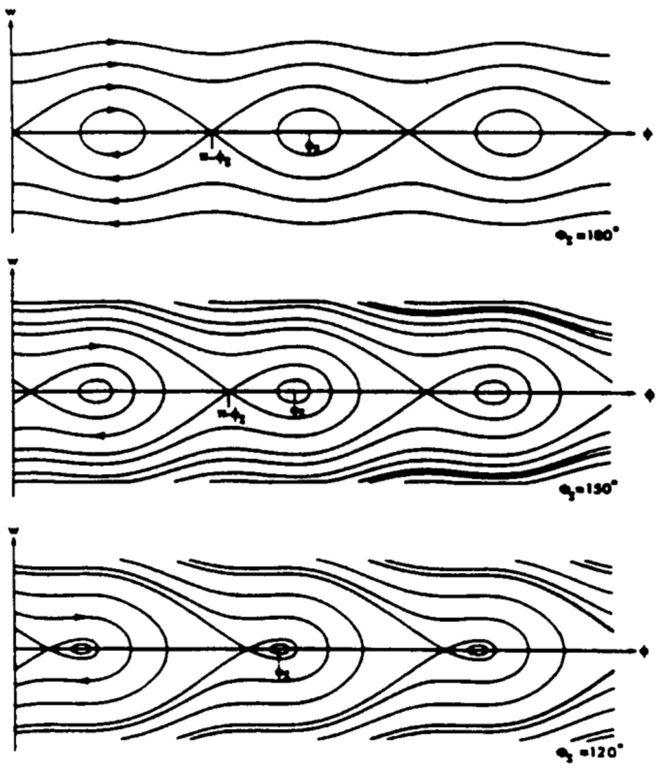

Figure 4.9: The buckets around the ring shrink during acceleration when the synchronous phase is moved towards 90°[32]

which translate into an acceptance in energy

$$\left(\frac{\Delta E}{E_s}\right) = \pm\beta\sqrt{-\frac{eV}{\pi h \eta E_s}G(\phi_s)}, \tag{4.91}$$

where

$$G(\phi_s) = 2\cos\phi_s + (2\phi_s - \pi)\sin\phi_s. \tag{4.92}$$

This RF acceptance strongly depends on ϕ_s and for a stationary bucket, there is no acceleration and $\sin\phi_s = 0$, so that $\phi_s = 0$ *or* π and consequently the maximum energy deviation by the RF-cavity with volatge U can be written as[32]

$$\Delta E_{max} = \pm\sqrt{\frac{2\beta^2 eUE}{\pi q(\alpha_c - \frac{1}{\gamma^2})}} \tag{4.93}$$

where α_c is the momentum compaction factor. It can be noted that the energy acceptance has the momentum compaction factor in the denominator which depends purely on the lattice parameters. The momentum compaction relates the path length of a particle in the ring to its energy deviation

$$\frac{\Delta p}{p}\alpha_c = \frac{\Delta L}{L}.$$

For strong focusing lattices, the momentum compaction factor is a small number and thereby increases the momentum acceptance. A small momentum compaction factor, however, also leads to lower thresholds for beam instabilities. Hence, if this maximum energy deviation ΔE_{max} is greater than the maximum energy loss ϵ_{max}, then particles will not be lost because the threshold for longitudinal momentum acceptance will be large enough that particles after losing maximum energy, will not hit the vacuum chamber and will be brought back to stable region by the RF cavity. However, dynamical longitudinal acceptance dependance can be measured through geometrical shape of a beam chamber and a maximum transverse dispersion such as

$$\delta_{acc}^{D} = \frac{r}{D_{max}}$$

where δ_{acc}^{D} is dynamical longitudinal acceptance, r is radius of beam chamber and D_{max} is maximum dispersion. This dynamical longitudinal acceptance should also be considered especially in the storage ring. Thus, to make sure that particles are moving out of longitudinal acceptance, both types of longitudinal accpetance should be considered.

4.3.4 Intrabeam Scattering (IBS)

Besides the beam-target effects, intrabeam scattering (IBS) is the most important cause of beam losses. The individual particles of a charged particle beam circulating in a storage ring occasionally scatter on one another. The IBS is due to the Coulomb interaction between the beam particles. The focusing forces and the RF accelerator voltage of the storage ring play an important role to keep particles alive. Due to the dispersion a change in energy always causes a change in the betatron amplitude, and a coupling arises between the synchrotron oscillation and the betatron oscillation. Furthermore, above transition energy the particles behave as if they had a negative mass, i.e. an increase of energy reduces the revolution frequency. Due to this behaviour, an equilibrium distribution of protons cannot exist above transition energy and the IBS will increase all in three dimensions of the bunch in so far as they do not hit other limitations. But even when an equilibrium distribution exists (below transition energy) the initial distribution will, in general, be different from the equilibrium distribution and the change of the distribution due to the IBS can reduce the beam lifetime in the storage ring. [33]

Particles within a bunch can scatter with each other as they perform betatron and synchrotron oscillations. The collisions lead to a redistribution of the momenta within the bunch, and hence to a change in the emittances. If a collision results in the transfer of transverse to longitudinal momentum at a location where the dispersion is non-zero, the result (after many scattering events) can be an increase in both transverse and longitudinal emittance, in a way similar to the increase in emittance by quantum excitation. A large change in momentum ("large-angle scattering") can lead to the energy deviation of particles becoming larger than the energy acceptance of the ring, in which case the particles will be lost. This is the **Touschek effect**, which limits the lifetime of the beam[34].

An internal beam is assumed where the longitudinal velocity spread is small compared to the transverse velocity spread, *i.e.*, the longitudinal temperature of the cooled particles is much smaller than the transverse one, $Temp_l << Temp_{tr.}$. in other words, the RMS width of the relative momentum deviation δ is very small. The longitudinal heating, *i.e.*, the rate of change of δ^2, is described by

$$D_{\parallel}^{IBS} = \frac{\Lambda_{\parallel}^{IBS}}{\epsilon_{\perp}^{3/2}}, \quad \Lambda_{\parallel}^{IBS} = \frac{\sqrt{\pi N_i c r_i^2 L_c}}{4\gamma_0^3 \beta_0^3 \langle\sqrt{\beta_{\perp}}\rangle C} \tag{4.94}$$

where N_i is the number of circulating ions, c is the speed of light, $L_c \approx 10$ is the Coulomb logarithm, $\beta\gamma$ is beam momentum, $\langle\sqrt{\beta_{\perp}}\rangle$ the average of the sqaure root of the betatron amplitudes in the ring, C is the ring's circumference and r_p is the classical proton radius and $\epsilon_{\perp} = \sqrt{\epsilon_x \epsilon_y}$ a measure of the horizontal and vertical rms beam emittance[28]. The corresponding beam loss rate is related to the mean square relative momentum deviation

$$\frac{1}{\tau_{loss}} = \frac{D_{\parallel}^{IBS}}{L_c \delta_{cut}^2}. \tag{4.95}$$

where δ_{cut} is the longitudinal ring acceptance. For a given beam momentum the loss rate due to Touschek is proportional to the number N_i of circulating particles and inversely proportional to $\epsilon_{\perp}^{3/2}$ and $\beta^3\gamma^3$[27].

4.3.5 Total loss rate

The total loss rate is just the sum of individual loss rates,[27]

$$\frac{1}{\tau_{loss}} = \frac{1}{\tau_{loss,h}} + \frac{1}{\tau_{loss,c}} + \frac{1}{\tau_{loss,E}} + \frac{1}{\tau_{loss,ibs}} \tag{4.96}$$

where, $1/\tau_{loss,h}$ denotes the loss rate due to the total hadronic cross section, $1/\tau_{loss,c}$ the loss rate due to the large angle single Coulomb scattering, $1/\tau_{loss,E}$ the loss rate due to the finite relative momentum acceptance δ_{cut} and $1/\tau_{loss,ibs}$ the loss rate due to the Touschek effect. The beam lifetime τ can be calculated by taking reciprocal of $1/\tau_{loss}$. Beam lifetimes at low momenta strongly depend on the beam cooling scenario and ring acceptance. The beam loss rate for single Coulomb scattering could significantly be reduced by applying a larger electron beam diameter in combination with stochastic cooling.

CHAPTER 5

Beam Simulation Results

There are many simulation codes which are used for simulation of accelerator physics especially to study particle motion inside accelerator machines. For the PTR, lattice optics is studied through the usage of *Methodical Accelerator Design* MAD-X [2]. MAD-X is a tool, built by the CERN community, for charged-particle optics design and studies in alternating-gradient accelerators and beam lines for general purpose. It can be handled for different sizes of accelerators, ranging from medium size to large. As every accelerator simulation software has built-in and customized options for elements, customization of elements is used for PTR because MAD-X was built for conventional accelerator ring designs which contains all magnetic elements. In the MAD-X manual, definitions for all related beam dynamics and structures of all elements are discussed in details, however, the definition of disperision concerning this work, needs a little clarification. As *dispersion* in MAD-X is defined by the following expression

$$D = \frac{d(x,y,s)}{dpt} \quad \text{where} \quad pt = \beta\frac{\Delta p}{p} \tag{5.1}$$

however, the convential defintion of *Dispersion* is considered as

$$D = \frac{d(x,y,s)}{\frac{\Delta p}{p}}.$$

For sake of easiness, dispersion will be considered as deifned in Eq.(5.1).

After generating the lattice optics for the PTR, the beam losses are calculated using the analytical formulas given in chapter 4. These calculations are performed by using *Wolfram Mathematica*[3], a symbolic mathematical computation program.

5.1 Ring Design

As alreday mentioned in chapter 3 the PTR will be a squared ring with four periodic cells and each cell will consist of focusing, defocusing and bending elements along with drift elements. For smooth and better implemetation, the cells are precisely arranged into the following structure for MAD-X

$$SSQ - D - QF - D - EB - D - QD - D - EB - D - QF - D - SSQ$$

where SSQ is a straight section quadrupole, D is a drift section and EB stands for electrostatic bending elements and QF,QD are for focusing and defocusing quadrupoles. According to a preliminary design of the PTR, discussed in chapter 3, which allows to add only electrostatic deflectors 'EB' elements by adding transfer matrix for lattice optics generation. Section 4.2 explains in details the derivation of transfer matrices which will be calculated for the PTR in next section.

For lattice design and optics, the PTR all electric mode parameters given in Tables 3.1 and 3.2 are used.

5.2 Transfer Matrices for Electrostatic Deflector

A pure electric bending element is defined in MAD-X by a transfer matrix which is derived in section 4.2. Specific calculation of matrix elements for the PTR are done here by considering geometrical prameters of bending shown in Table 5.1.

Parameter	Value	Unit
No. of Bends	16	
Deflector length	3.4795	m
Bending Radius	8.861	m
Horizontal gap	60	mm
Vertical gap	150.6	mm
Potential between plates	200	kV

Table 5.1: Bending Parameters

After substituting all parameter values in Eq.(4.69), the first order matrix with cylindrical bending shape with $\eta = 0$ and $\xi = \sqrt{2}$ and considering straight non-bending side ($i.e.$ $R_y = 0$), is given below

$$EB = \begin{bmatrix} 0.85418 & 3.30871 & 0 & 0 & 0 & 1.29205 \\ -0.0817166 & 0.85418 & 0 & 0 & 0 & 0.724056 \\ 0 & 0 & 1 & 3.47954 & 0 & 0 \\ 0 & 0 & 0 & 1 & 0 & 0 \\ -0.724056 & -1.29205 & 0 & 0 & 1 & 2.94856 \\ 0 & 0 & 0 & 0 & 0 & 1 \end{bmatrix}$$

5.3 Lattice Study

The first task of this thesis is to generate PTR lattice optics for the 30 MeV mode because optimized lattice optics can help to reduce systematic errors and increase beam lifetime in the storage ring. The flexibility of the lattice also allows to consider a wide range of betatron tunes (see section 5.3.2).

5.3.1 Optical Functions

Optical functions (such as β_x, β_y and D_x) decribe the particle motion in the ring. These functions depend on position s in the ring. Since the quadrupoles have different strengths and are not located homogeneously around the ring, the optical functions vary as a function of s. In the PTR design, the vertical betatron function β_y defines the focusing strength which does vary over a large range for differnt quadrupole strengths in the lattice. Therefore, to find an optimal lattice, study of more than one lattice is needed and for that purpose, four different lattices are considered in this thesis with different initial focusing. The following types of lattices will remain under discussion for the rest of the thesis

(i) Strong Focusing with $\beta_{y-max} = 33\,\text{m}$

(ii) Medium Focusing with $\beta_{y-max} = 100\,\text{m}$

(iii) Weak Focusing with $\beta_{y-max} = 200\,\text{m}$

(iv) Weaker Focusing with $\beta_{y-max} = 300\,\text{m}$

The effects which appear due to different types of focusing are also studied by calculating beam losses discussed in detail in chapter 5.4.

1) Strong Focusing:

When it is compared with other lattices mentioned above, the focusing strength with $\beta_{y-max} = 33\,\text{m}$ is labelled as strong focusing. Though, there is a possibility to make focusing strength even stronger, but the reason to consider it as stronger, are the betatron tunes Q_x, Q_y which are in a range of the acceptance by the accelerator physicists. Therefore, betatron tunes for this lattice along with all others values which may change by changing focusing strength and may have impacts on beam losses, are mentioned in Table 5.2 below and lattice optics also shown in Figure 5.1.

Parameter	value
Maximum vertical β_{y-max}	33.48 m
Maximum horizontal β_{x-max}	11.67 m
Maximum horizontal dispersion D_{x-max}	11.92 m
Momentum compaction α_c	0.5549
Transition energy γ_{tr}	1.342
Horizontal tune Q_x	1.75
Vertical tune Q_y	1.22

Table 5.2: Lattice parameters

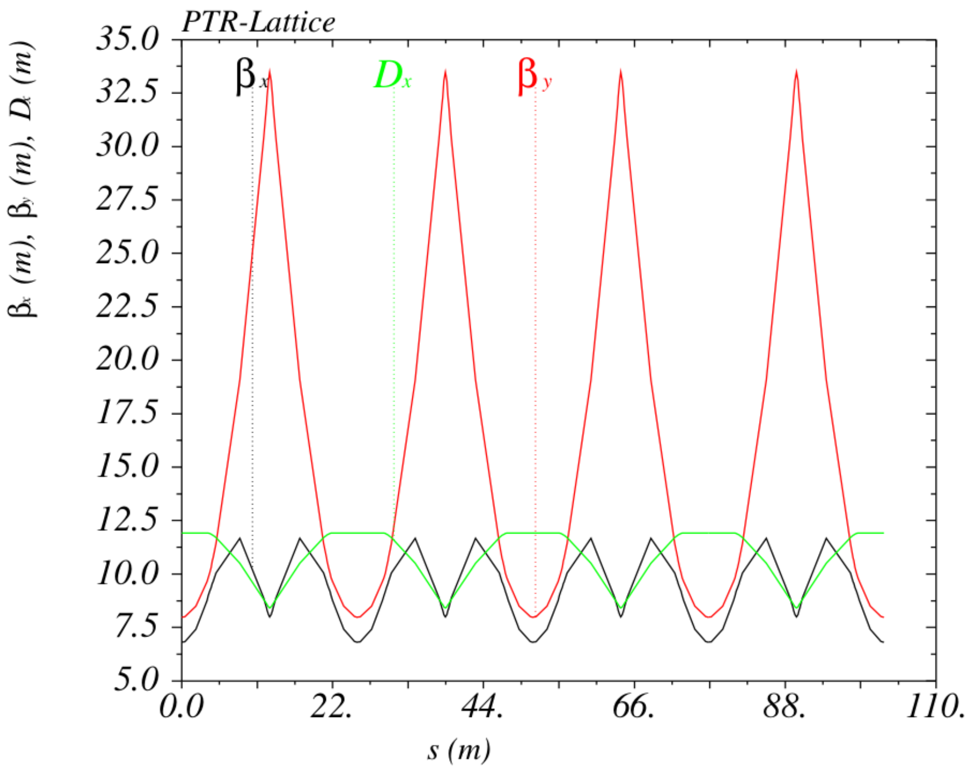

Figure 5.1: Beta functions $\beta_y(red), \beta_x(black)$ and horizontal dispersion $D_x(green)$ vs circumference of ring s.

The betatron functions and dispersion change continuously along the ring, but in the above table only the maximum values are mentioned. α_c and γ_{tr} plays role in the beam losses. This lattice will be referred to as the *Standard Lattice* from this point to onwards.

2) Medium Focusing:

The second lattice is generated by adjusting the quadrupole strengths and tune β_{y-max} to 100 m. This lattice is labelled as *"Medium focusing"*. The behaviour in variation of betatron functions and dispersion is same as for the first lattice and the optical functions of this lattice are shown in Figure 5.2 and all important parameters are shown in Table 5.3

Parameter	value
Maximum vertical β_{y-max}	100.05 m
Maximum horizontal β_{x-max}	14.34 m
Maximum horizontal dispersion D_{x-max}	11.59 m
Momentum compaction α_c	0.546
Transition energy γ_{tr}	1.353
Horizontal tune Q_x	1.83
Vertical tune Q_y	1.75

Table 5.3: Lattice parameters

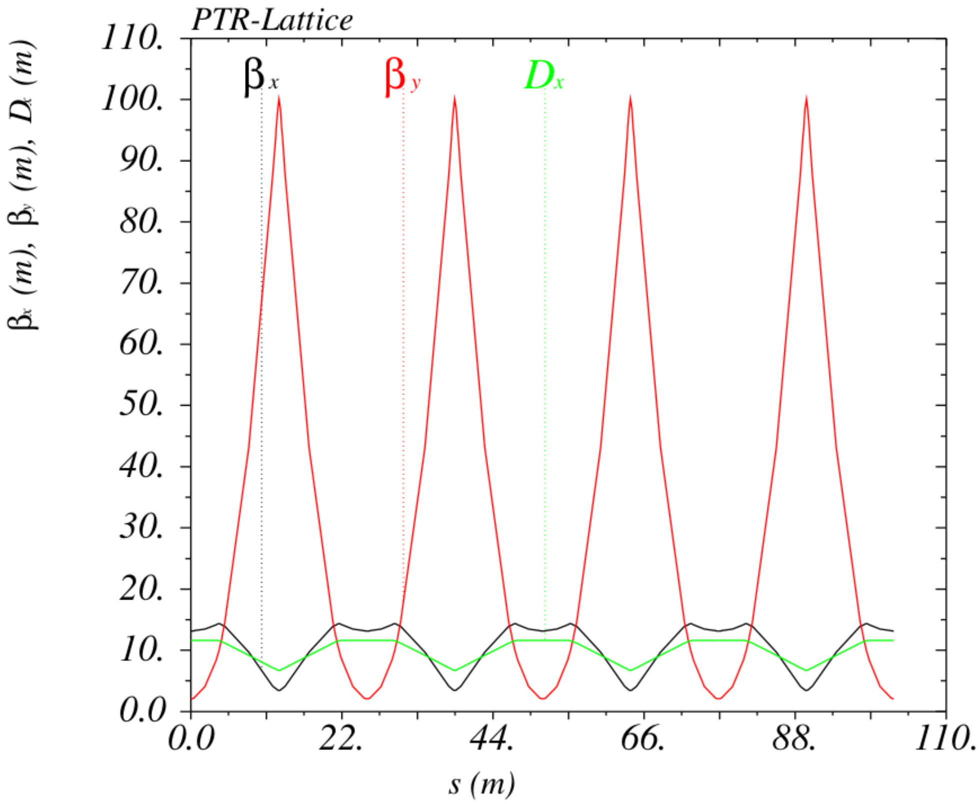

Figure 5.2: Beta functions $\beta_y(red), \beta_x(black)$ and horizontal dispersion $D_x(green)$ vs circumference of ring s

From Table 5.3, it can be seen that the vertical betatron function varies prominently however horizontal betatron function does not vary much. The difference between both betatron functions make clear that it is a vertical focusing lattice where horizontal dispersion does not change and remains almost the same when compared to the first lattice. There is a slight change in the momentum compaction factor and transition energy but the vertical betatron tune changes more than the horizontal one.

3) Weak Focusing:

The third lattice is generated by adjusting the quadrupole strengths to bring vertical betatron function value at $\beta_{y-max} = 200\,\text{m}$. This lattice is labelled as *"Weak focusing"* because particles have a large vertical amplitude and are not focused fully towards the reference beam motion. The behaviour in variation of the betatron functions and dispersion is the same as for first two lattices and the optical functions of this lattice are shown in Figure 5.3 and all important parameters are shown in Table 5.4

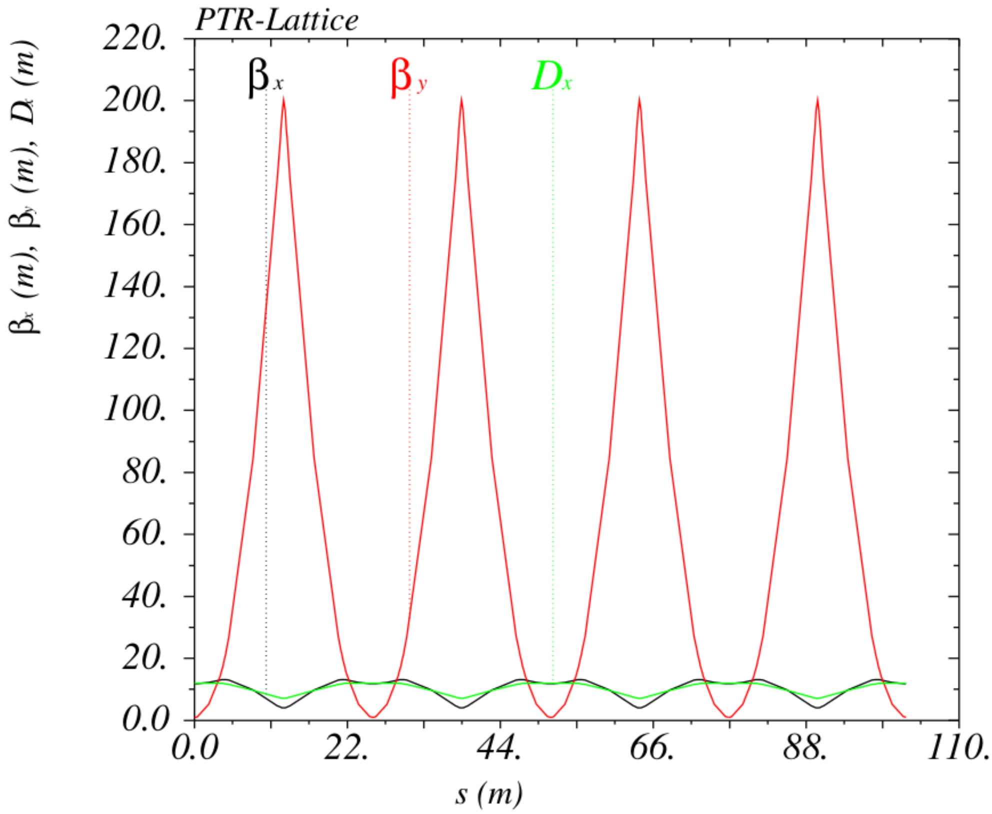

Figure 5.3: Beta functions $\beta_y(red), \beta_x(black)$ and horizontal dispersion $D_x(green)$ vs circumference of ring s

Parameter	value
Maximum vertical β_{y-max}	200.09 m
Maximum horizontal β_{x-max}	13.17 m
Maximum horizontal dispersion D_{x-max}	11.93 m
Momentum compaction α_c	0.549
Transition energy γ_{tr}	1.349
Horizontal tune Q_x	1.79
Vertical tune Q_y	1.88

Table 5.4: Lattice parameters

It is visible from the lattice optics and their maximum values that the main difference appears in the vertical motion of particles. However, the horizontal beta β_x and dispersion D_x do change but slightly and the same behaviour can be seen in other parameters.

4) Weaker Focusing:

The fourth and last lattice is generated by adjusting the quadrupole strengths to bring the vertical betatron function value at $\beta_{y-max} = 300$ m. This lattice is labelled as *"Weaker focusing"* because particles have larger vertical amplitude and are not focused fully towards the reference beam motion. The behaviour in variation of betatron functions and dispersion is the same as for the first three lattices and the optical functions of this lattice are shown in Figure 5.4 and all important parameters are shown in Table 5.3.1

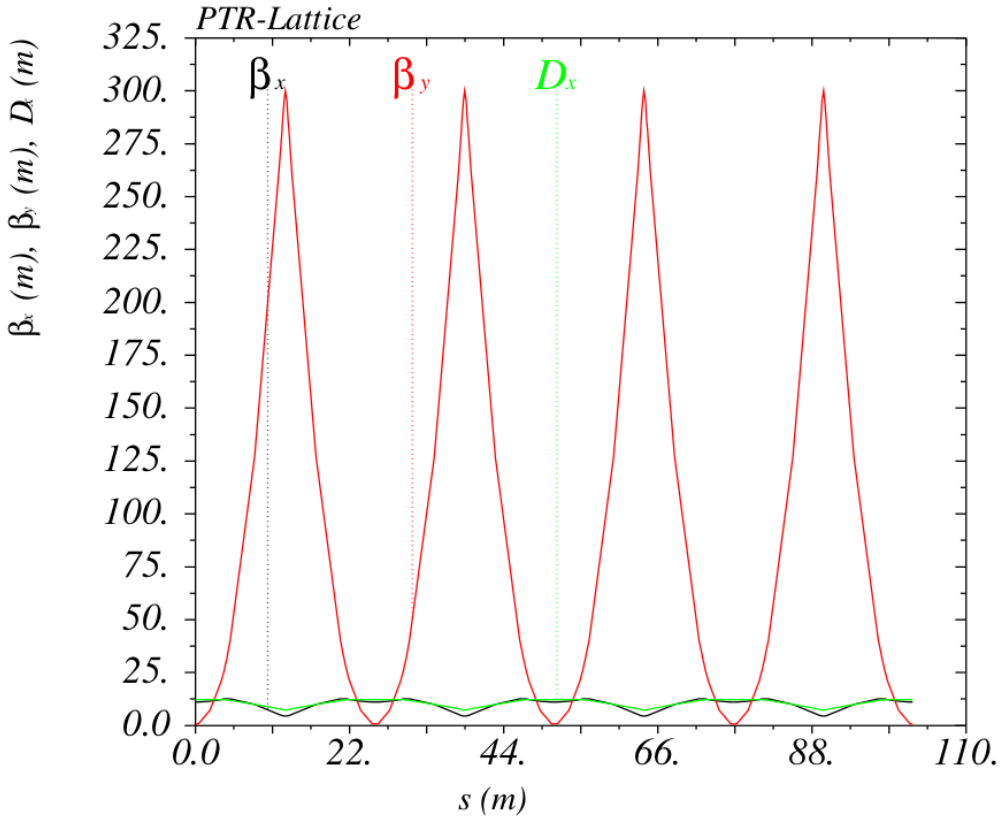

Figure 5.4: Beta functions $\beta_y(red), \beta_x(black)$ and horizontal dispersion $D_x(green)$ vs circumference of ring s

Parameter	value
Maximum vertical β_{y-max}	300.07 m
Maximum horizontal β_{x-max}	12.55 m
Maximum horizontal dispersion D_{x-max}	12.16 m
Momentum compaction α_c	0.551
Transition energy γ_{tr}	1.347
Horizontal tune Q_x	1.77
Vertical tune Q_y	1.92

Table 5.5: Lattice parameters

Once again, the vertical betatron function much larger than horizontal in amplitude. Both horizontal β_x and D_x have almost the same maximum magnitude and the vertical betatron tune is greater than the horizontal one and one can notice that it is not true for the first two lattices *i.e.*, in the strong and medium lattices.

For this thesis, only four lattices are being considered with large vertical focusing differences but how far one can change the quadrupole strengths to get different types of lattices? The answer lies in the below section of tune variability which tells about how flexible the lattice is.

5.3.2 Tune Variability

The flexibility of this PTR lattice structure helped to generate different types of lattices having different betatron tunes. This betatron tunes variation can be seen by considering all possible quadrupoles strengths which keep the beam in the closed orbit. This is done in two steps. The first step is to keep the straight section qaudrupole (SSQ) off ($Kss = 0$)and put the defocusing quadrupoles at some fixed value (let's take $KQd = 0.3\,/\mathrm{m}^2$). Then the focusing quadrupoles are varied step by step. This can be seen in Figure 5.5

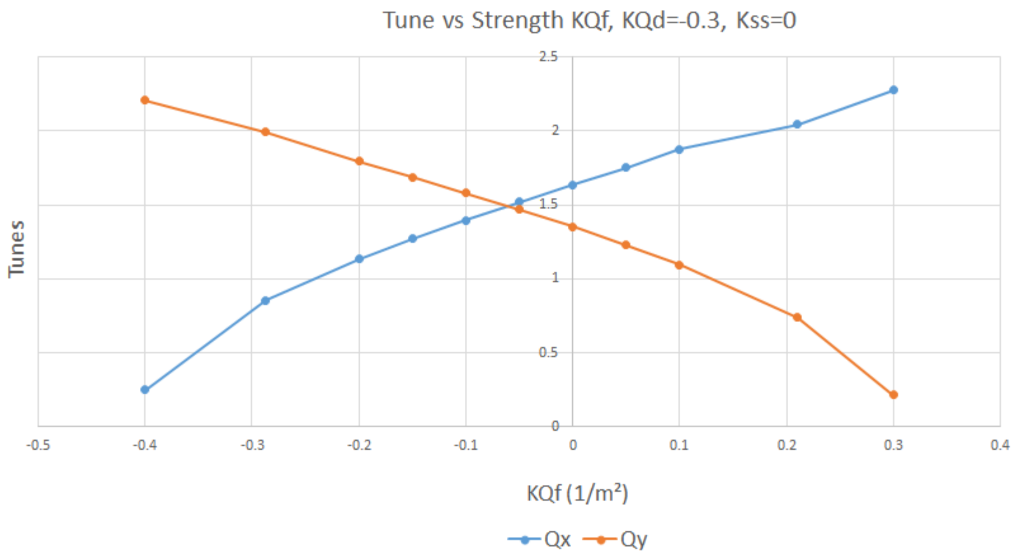

Figure 5.5: Betatron tunes variation with focusing quadrupole strength

The second step of further betatron tunes variation is by keeping focusing quadrupole strength constant (let's consider standard lattice betatron values in Figure 5.5 with $kQf = 0.05$ and $KQd = -0.3$) and turning on the straight section quadrupoles and vary their strengths to see how smooth the optical functions can be made. This tune behaviour is shown in Figure 5.6

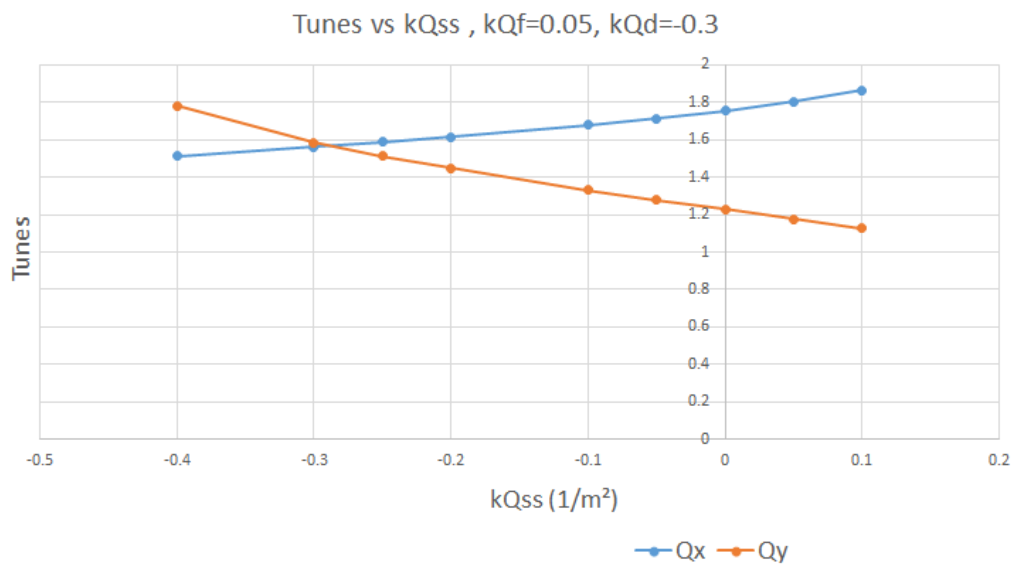

Figure 5.6: Betatron tunes variation with focusing strength of straight section quadrupole

Thus, it can be observed that the betatron tunes of this lattice design varies for Q_x and Q_y between 0.2 to 2.4. This large variation with different combination of betatron tunes for different quadrupole strengths shows the flexibility of lattice design. A variety of lattices helps to find optimal lattice for PTR experiment with minimum systematic effects and maximum storage time in the ring.

5.4 Estimation of Beam losses

This section is about an estimation of beam losses by considering some of the main processes in the storage ring. The processes assist in the beam emittance blow-up, reduction of beam intensity and then resulting in particle losses are discussed below.

Main Effects of Beam Losses

Due to the high requirement concerning the beam stability and the beam lifetime, all main beam loss effects at low energy are needed to be investigated. The calculations of beam loss rates are done by using analytical formulas which are discussed in detail in section 4.3. These effects are studied with a target which would detect the polarized beam and without target by considering only residual gas that is a combined mixture of hydrogen H_2 and nitrogen N_2 gases. In the following sections, estimations of beam loss rates from the main effects and dependencies of the beam lifetime on the target thickness and longitudinal acceptance are also studied.

5.4.1 Hadronic Interactions

This type of inteactions depend on the cross section of interaction particles, therefore two different cases will be investigated for proton beam.

With Residual Gas

The general formula to calculate the beam loss rate Eq.(4.74) which shows a dependency on the total hadronic cross section area σ_{total} and the desity of particles as well as velocity of the revoloving particles which in this case are protons. As residual gas is a composition of hydrogen and nitrogen gases with a fraction of 80:20 respectively. Individual cross section of proton to hydrogen σ_{pH} and proton to nitrogen σ_{pN} are taken from [35]. The values are related to a beam energy of 30 MeV where the velocity $v = c\beta$ for the proton is $v = 7.4 \times 10^7\,\mathrm{m\,s^{-1}}$. However, for a composite gas an effective total cross section is useful for the beam loss rate which can be obtained by multiplying fraction of each gas with its cross sectional area and summing up all resulting cross sections.

$$\sigma_{pH} = 139\,\mathrm{mb} \quad , \quad \sigma_{pN} = 465\,\mathrm{mb}$$
$$\sigma_{total} = \sigma_{pH} f_{H_2} + \sigma_{pN} f_{H_3} = 204\,\mathrm{mb}$$

where the fractional ratio of hydrogen and nitrogen gas is $f_{H_2} = 0.8$ and $f_{N_2} = 0.2$ and the density n of the rest gas particles is calculated by Eq.(4.75). In the present case, P_{eq} is N_2 equivalent pressure which is $P_{N_2,eq} = 2.8 \times 10^{-11}$ Torr and the resulting density of the rest gas is $n = 1.9 \times 10^6$ atoms per volume. Thus substituting these values into Eq.(4.74) gives

$$\frac{1}{\tau_{HI}^{rg}} = vn\sigma_{tot} = 2.993 \times 10^{-15}\,\mathrm{s^{-1}}. \tag{5.2}$$

This is an estimation of the beam loss rate which contributes from hadronic interactions only in the absence of a target. It is very small because of very low pressure however by increasing pressure, the density of the rest gas particles also increases which enhances the beam loss rate and consequentely reduces the beam lifetime.

With Target

The presence of a target inside the vacuum tube overshadows the beam loss rates due to rest gas. In the present case, target is a hydrogen pellet with a density of $n_t = 4.0 \times 10^{15}\,\mathrm{atoms/cm^2}$ and the total cross section at $T = 30\,\mathrm{MeV}$ is $\sigma_{pp} = 85\,\mathrm{mb}$ taken from [36]. The revolution frequency of proton beam is $f_0 = 1.138\,\mathrm{MHz}$. Thus, after substituting these values in the beam loss rate Eq.(4.74) delivers

$$\frac{1}{\tau_{HI}^{t}} = f_0 n_t \sigma_{pp} = 3.869 \times 10^{-7}\,\mathrm{s^{-1}}. \tag{5.3}$$

Thus the total beam loss rate due to hadronic interactions in the presence of a residual gas and a target is obtained adding Eq.(5.2) and Eq.(5.3) which brings the following value

$$\frac{1}{\tau_{HI}^{tot}} = 3.869 \times 10^{-7}\,\mathrm{s^{-1}}. \tag{5.4}$$

As expected, the hydrogen pellet target predominantly effects the beam loss rate and reduces the beam lifetime. As there is no dependency on optical functions values, therefore Eq.(5.4) will remain same for all lattices.

5.4.2 Coulomb Scattering

The Coulomb scattering can be calculated for single and multiple Coulomb scattering. But if single or multiple scattering angles larger than beam pipe, then these scattering angles should be restricted by ring transverse aperture. Two different cases, with a target and with only residual gas, are estimated by restricting the transverse aperture for scattering angles.

With Residual Gas

Elastic scattering processes are considered by ignoring screening effects by shell electrons and mathematical divergency problems at very small scattering angles. Therefore classical Rutherford scattering with the differential cross section σ_{tot} given in Eq.(4.77) is considered here. The expression given in Eq.(4.74) for beam loss rate $1/\tau_{loss}$ due to elastic Coulomb scattering is written after substituting Eq.(4.77) and Eq.(4.75) for two gasses (*i.e.*, H_2 and N_2) as,

$$\frac{1}{\tau_{cs}} = c\beta 2A \frac{\sum_t P_t Z_t^2}{760} \left(\frac{z_i^2 e^8}{4\beta^2 (cp)^2} \frac{4\pi}{(\frac{\theta_{acc}}{2})^2} \right). \tag{5.5}$$

where $z_i = 1$ for the proton with $\beta = 0.247$, momentum $cp = 239.158\,\mathrm{MeV}$ and P_t Z_t is the partial pressure and atomic number of particles of the residual gas atoms. For calculations, residual gasses with their partial pressures and atomic number are given in Table 5.6.

Element	Patial pressure $P_j(Torr)$	Atomic number Z_j
H_2	6.46×10^{-10}	1
N_2	5.70×10^{-13}	7

Table 5.6: Rest gases with partial pressure and atomic number.

However, θ_{acc} in Eq.(5.5) is calculated by the transverse momentum acceptance A and the average beta-function $\langle\beta_\perp\rangle$ as

$$\theta_{acc} = \sqrt{\frac{A}{\beta_\perp}}.$$

For the PTR, the transverse acceptance is $A_{trns} = 10\,\mathrm{mm\,mrad}$ and the average betatron function $\langle\beta_\perp\rangle$ depends on the type of optics. So for all lattices, the average beta functions and resulting scattering angles are given in Table 5.7.

Lattice type	$\langle\beta_\perp\rangle$(m)	θ_{acc}(rad)
Strong	12.206	9.051×10^{-4}
Medium	21.560	6.810×10^{-4}
Weak	36.312	5.247×10^{-4}
Weaker	51.535	4.405×10^{-4}

Table 5.7: Average betatron function values and resulting scattering angles for all four lattices

Thus, the estimation of the beam losses in all lattices are given in Table 5.8

Lattice type	$1/\tau_{loss}$ (s^{-1})
Strong	4.274×10^{-31}
Medium	7.549×10^{-31}
Weak	1.271×10^{-30}
Weaker	1.804×10^{-30}

Table 5.8: Beam losses due to rest gas for all four lattices

It can be seen that the effect of beam losses due to Coulomb scattering is low with rest gas due much lower pressure, however by increasing partial pressures and considering more than two gases mixture, also effects beam loss rate. The dependency of pressure on the beam lifetime can be visualized in Figure 5.7,

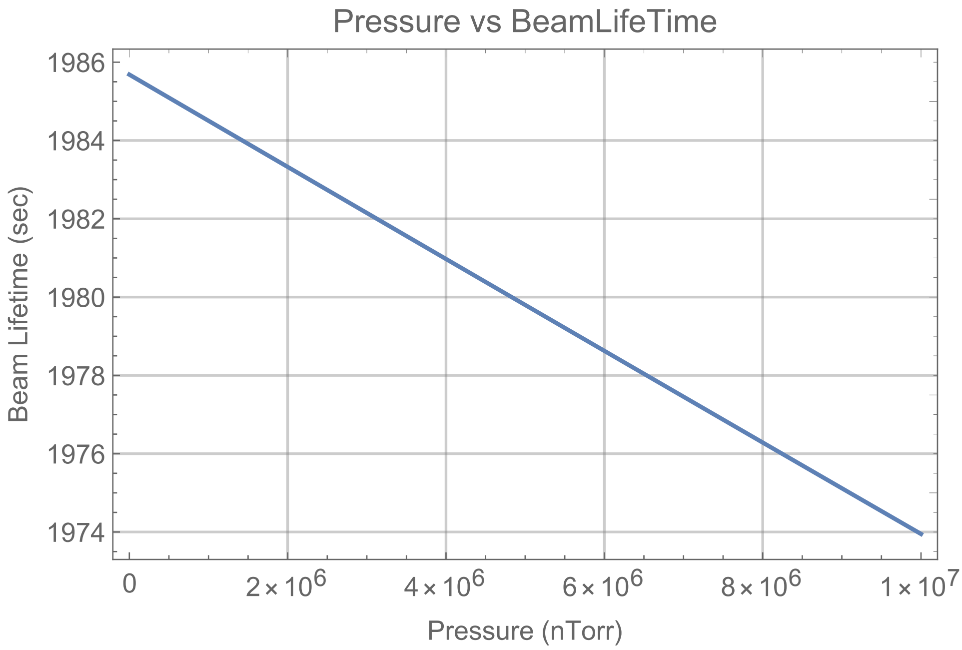

Figure 5.7: Pressure vs Beam Lifetime

With Target

The presence of a target in the path of beam changes the beam loss rate. The Eq.(4.74) is again considered but now the Rutherford cross-section is included,resulting in

$$\sigma_{tot} = \frac{4\pi z_i^2 Z_t^2 r_p^2}{\beta^4 \gamma^2 \theta_{min}^2}$$

where $Z_t = z_i = 1$, $\gamma = 1.032$ and θ_{min} is alreday given in Table 5.7 for all lattices. After subsituting all values, the total beam loss rate due to Coulomb scattering with a target presence for all lattices, is shown in Table 5.9.

Lattice type	$1/\tau_{loss}$ (s^{-1})
Strong	4.151×10^{-4}
Medium	7.332×10^{-4}
Weak	1.235×10^{-3}
Weaker	1.752×10^{-3}

Table 5.9: Beam losses due to a target for all four lattices

This rate is much larger than, the rate due to rest gas particles.The total contribution in the presence of the rest gas and a target is obtained by adding the above individual results for both cases for all lattices separately, which is summarized in Table 5.10

Lattice type	$1/\tau_{loss}$ (s^{-1})
Strong	4.151×10^{-4}
Medium	7.332×10^{-4}
Weak	1.235×10^{-3}
Weaker	1.752×10^{-3}

Table 5.10: Beam losses due to a target and rest gas for all four lattices.

Comparing the two effects, losses due to a target are much more prominent than due to the residual gas. If the target thickness changes, the beam lifetime changes as well dramatically which can be seen below in Figure 5.8.

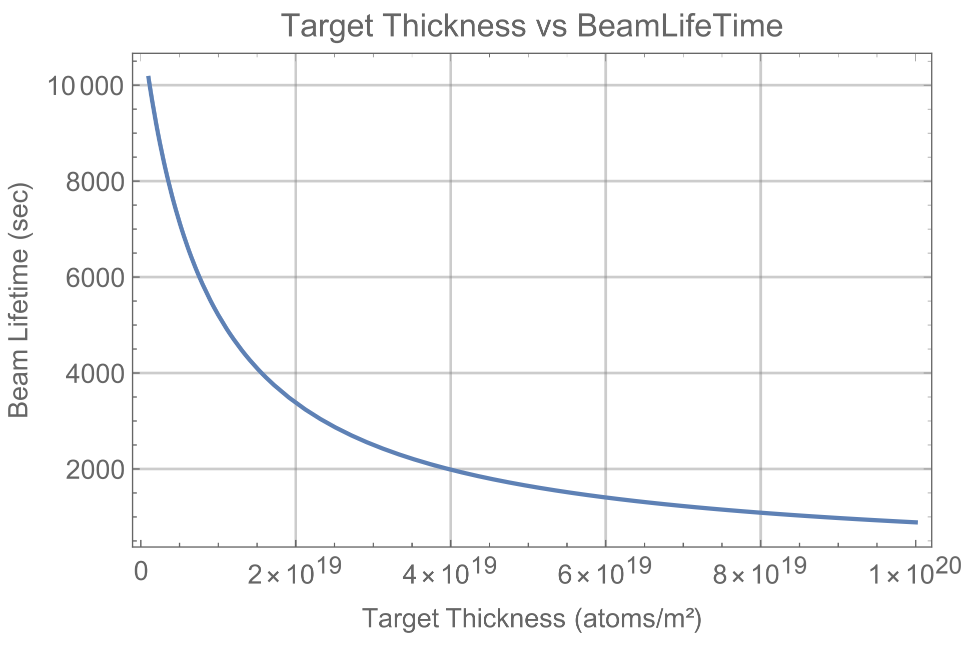

Figure 5.8: Target Thickness vs Beam Lifetime

Hence, it is clear if the target thickness increases, more particles get lost in the ring.

5.4.3 Energy Loss Straggling

Energy loss due to beam-target interaction out of the longitudinal acceptance δ_{acc} of the accelerator leads to beam losses. The single collision energy loss probability P_{loss} (with energy loss ϵ) is calculated by Eq.(4.86). The maximum energy loss in a collision with target particles (ϵ_{max}) for the PTR is calculated by Eq.(4.82). which results in

$$\epsilon_{max} = 66.32\,\text{keV}.$$

Thus, the resulting maximum longitudinal momentum deviation given by Eq.(4.83) yields

$$\delta_{max} = 1.12 \times 10^{-3}.$$

For energy losses, this δ_{max} should be greater than the geometrical longitudinal acceptance δ_{acc} which is calculated at a point where the dispersion is maximum. For the PTR, the chambar radius is $r = 30 \times 10^{-3}$ m. Thus,

$$\delta_{acc} = \frac{30 \times 10^{-3}\,\text{m}}{D_{max}}$$

where D_{max} is the maximum dispersion varies for different lattice optics. Table 5.11 shows the maximum geometrical longitudinal acceptance for all four types of lattices of the PTR.

Lattice type	δ_{acc}
Strong	2.519×10^{-3}
Medium	2.588×10^{-3}
Weak	2.514×10^{-3}
Weaker	2.466×10^{-3}

Table 5.11: Maximum geometrical longitudinal acceptance for all four lattices.

It can be seen clearly that δ_{max} which corresponds to the maximum energy loss ϵ_{max} is smaller than the allowable longitudinal accpetance calculated in Table 5.11 for all lattice types *i.e.*, $\delta_{acc} > \delta_{max}$. Hence, all particles even after losing the maximum energy still stay within the stable region of the beam so there are no particle lost due to energy straggling. This effect can be crossed check by calculating the maximum energy deviation ΔE_{max} in the RF cavity which also deals with the longitudinal motion of the particles. This ΔE_{max} should be greater than ϵ_{max} so that particles remain inside bucket. The calculation of the maximum energy deviation is performed for the strong lattice and plotted against the phase ϕ as shown in Figure 5.9.

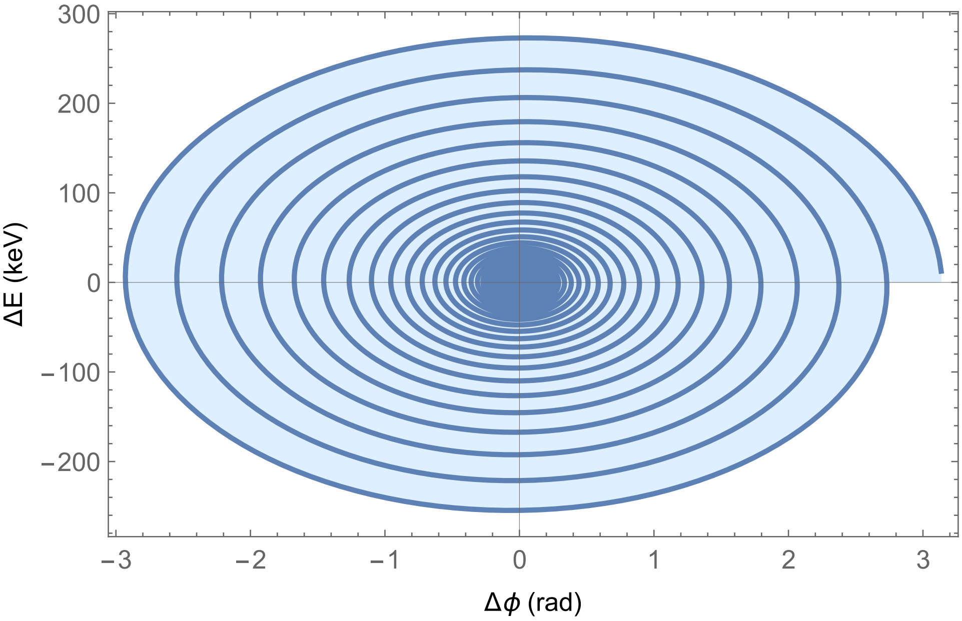

Figure 5.9: Maximum Energy Deviation vs Phase-angle ϕ.

It can be seen that, the maximum energy is more than 200 keV at $\Delta\phi = 0$ for which a particle can stay within the bucket. It means that after losing the maximum energy ϵ_{max} by an energy staggling process, the proton beam still remains in the RF-bucket and does not get lost. Therefore, in the beam loss probability Eq.(4.86) gives negative results which means nothing other that the probablity intergal isn't valid when allowable energy deviation is larger than the maximum energy loss. As longitudinal acceptance increases, more and more particles stay in the stable region and particles can be stored for a longer time, Figure 5.10 shows the longiudinal dependance on beam lifetime.

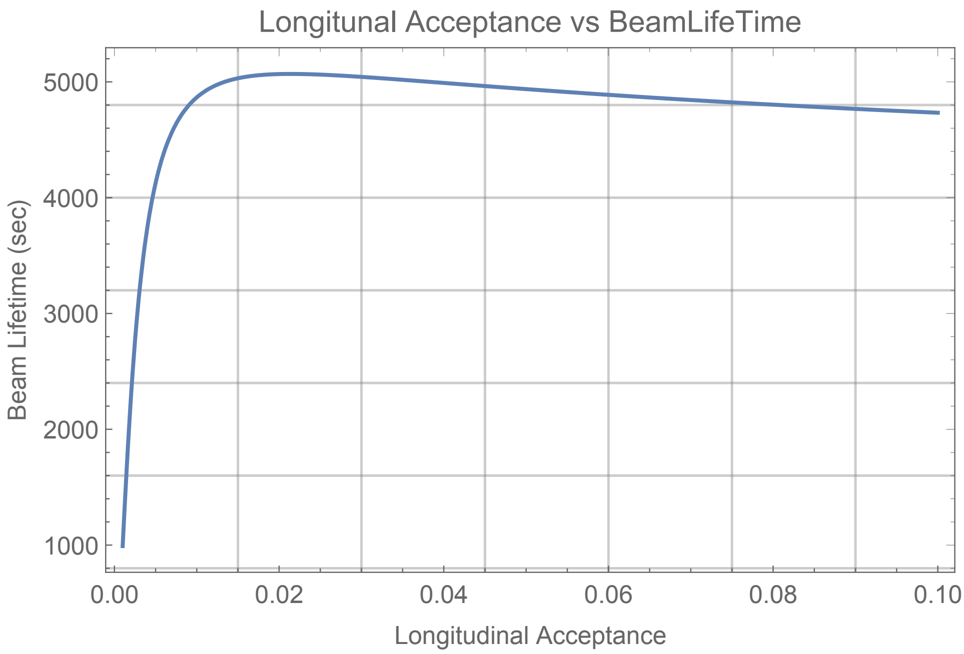

Figure 5.10: Maximum Geometrical Longitudinal Acceptance vs Beam Lifetime

For the PTR case with 30 MeV beam energy, the total beam losses due to energy starggling will be zero

$$\frac{1}{\tau_{ES}^{tot}} = 0\,\mathrm{s}^{-1}. \qquad (5.6)$$

5.4.4 Intra Beam Scattering (IBS)

Intrabeam scattering IBS is most dominant effect at low energy, especially large angle Coulomb scattering within beam particles which are studied under **"Touschek effect"**. Due to dependency of this effect on the beam density, transverse emittance and betatron function, the beam loss rate is free from target or residual gas presence. The beam loss rate is determined by the longitudinal diffusion coefficient $D_{\parallel}^{IBS}$ and the relative momentum acceptance δ_{max} calculated for all optics in Table 5.11.

The loss rate Eq.(4.95) is used here. The longitudinal diffusion coefficient is calculated for all optics using the average square root of the betatron amplitudes in the ring $\sqrt{\langle\beta_{\perp}\rangle}$ and the transverse emittance $\epsilon_{\perp} = \sqrt{\epsilon_x \epsilon_y} = 1\,\mathrm{mm\,mrad}$ as well as $N = 10^9$ particles in a beam. Table 5.12 shows the longitudinal diffusion coefficient $D_{\parallel}^{ibs}$ (analytical formula was given in Eq.(4.94) for all lattices and resulting the beam losses calculated by Eq.(4.95).

Lattice type	δ_{acc}	$D_{\parallel}^{ibs}$	$1/\tau_{loss}$ (s^{-1})
Strong	2.519×10^{-3}	5.592×10^{-10}	8.814×10^{-5}
Medium	2.588×10^{-3}	5.319×10^{-10}	7.942×10^{-5}
Weak	2.514×10^{-3}	4.757×10^{-10}	7.529×10^{-5}
Weaker	2.466×10^{-3}	4.381×10^{-10}	7.202×10^{-5}

Table 5.12: Diffusion coefficient and beam losses for all lattices.

It can be seen from the results that IBS is one of the most dominant effects which reduce the beam lifetime drastically. IBS does have more effects on the weaker lattice because as the vertical beta function increases, the average transverse beta function also increase which is directly proportional to the beam lifetime. However, the number of particles in a beam also effects beam lifetime as can be seen in the Figure 5.11

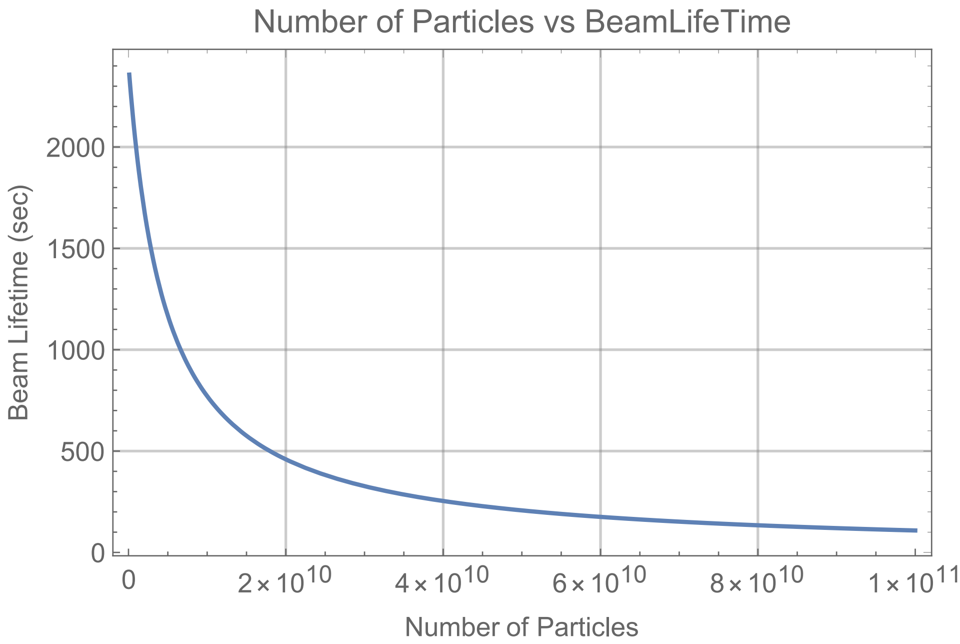

Figure 5.11: Number of Particles in a beam vs Beam Lifetime.

As the number of particles increses, more and more particles will interact and scatter and hit the beam chamber and therefore, the beam lifetime reduces.

5.4.5 Total Beam Loss Rate

After separate calculations of beam loss rates for all main effects, the total rate can be obtained just by linear addition of all rates as discussed in section 4.3.5. Therefore, the total beam loss rate and the beam lifetime which is just a reciprocal of beam loss rate for all four optics is given in Table 5.13.

Lattice type	$1/\tau_{total}$ (s^{-1})	τ_{total}(s)
Strong	5.3036×10^{-4}	1985.68
Medium	8.129×10^{-4}	1230.07
Weak	1.310×10^{-3}	763.09
Weaker	1.825×10^{-3}	547.98

Table 5.13: Total beam loss rate and resulting beam lifetime for all lattices.

As the focusing strength of the lattice is reduced, more and more beam losses are occuring which reduce the beam lifetime. The minimum time require for beam should be more than 1000 seconds which urges to choose a strong focusing lattice in which the beam lifetime is around 1985 seconds. However, more stronger lattices will give a higher beam lifetime but it will cause more systematic errors as well. This is the preliminary estimation of the lattice which gives an idea which type of lattice optics will be better for PTR. Nevertheless, to improve these results, dynamics of tail particles also need to be considered.

CHAPTER 6

Conclusion and Outlook

One of the many goals of the PTR is to reduce systematic effects in the EDM experiment by choosing a suitable lattice with reasonable focusing strength to enhance a high intensity beam lifetime. In this thesis, investiagations for a first mode of PTR with 30 MeV kinetic energy for protons with one beam circulation at a time, are done. The PTR lattice was simulated using MAD-X by introducing pure cylindrical electrostatic bending elements and studying different types of lattice for the PTR from weak to strong focusing. In addition, analytical calculations of the beam lifetime for four studied types of lattices were performed in Chapter 5. Only main effects of beam losses were remained under discussion in the last chapter which tell that the beam lifetime highly depends on the vacuum, the longitudinal and transverse acceptance momentum, the beam and target density, the transverse emittance and the focusing strength of the lattice. One of the most dominent effects of beam losses is intrabeam scattering (IBS) which depends on the average value of the betatron functions (β_x, β_y) and beam density.

Besides this, beam losses were considered under two different scenarios, *i.e*, **(a)** First, in the presence of the residual gas which contains only two most abundent gases, hydrogen H_2 and nitrogen N_2, with nitrogen equvialent pressure $P_{eq} = 2.8 \times 10^{-11}$ Torr and with the density of $n = 1.9 \times 10^6\,\mathrm{atoms/cm^3}$ and **(b)** Second with a target only, where the target was hydrogen pallet with a density of $n_t = 4.0 \times 10^{15}\,\mathrm{atoms/cm^2}$. After separate calculations of both cases, a combined calculation was performed which shows that the dominancy of the target on the beam lifetime is not compareable to the rest gas effects. This task was repeated for all types of lattices and the comparison gives a clue that the lattice with $\beta_{y-max} = 33\,\mathrm{m}$ is trade off between longer the beam lifetime and lesser the systematic effects. Eventually, the first analytical estimation with major beam losses effects and in the presence of a target along with the residaul gas, gives $\tau_{total} = 1985.68\,\mathrm{s}$ for the optimal lattice .

However, optimization of the PTR lattice is not at its peak and it needs more support from spin tracking analysis. Simulations for the second mode of the PTR , for example counter-rotating high intesity beams storage and shielding of magnetic fields at bending elements also need detailed studies. Electrostatic deflectors technique for the PTR, is under investigation at the IKP-Forschungszentrum Jülich. To reach a high EDM measurement precision at the final ring, the PTR is an important stage which can resolve many problems before construction of the final ring. Therefore, implementation of new concepts to measure the proton EDM at realistic grounds demands benchmarking of the PTR simulation to reduce maximum systematic errors. At Jülich, a dedicated group of people is putting its efforts to surprise the world by opening new door of possibilities in physics where many unanswerable questions would be answerable.

List of Figures

List of Tables

Bibliography

[1] A.D. Sakharov. Violation of CP Invariance, C Asymmetry, and Baryon Asymmetry of the Universe. *Soviet Physics Uspekhi*, 34(5):392–393, May 1991.

[2] H. Grote and F. Schmidt. CERN MADX introduction. `http://mad.web.cern.ch/mad/madx.old/Introduction/doc.html`, 2002.

[3] S. Wolfram. Wolfram Mathematica Computer program . `http://www.wolfram.com/?source=nav`, June 1988.

[4] JEDI collaboration F. Abusaif et al. Feasibility Study for an EDM Storage Ring. Technical Report arXiv:1812.08535, Forschungszentrum Jülich Germany, Dec 2018. * Temporary entry *.

[5] J.M. Pendlebury et al. Revised Experimental upper limit on the Electric Dipole Moment of the Neutron. *Phys. Rev. Lett.*, 92(9), Nov 2015.

[6] V. F. Dmitriev and R. A. Sen'kov. Schiff Moment of the Mercury Nucleus and the Proton Dipole Moment. *Phys. Rev. Lett.*, 91:212–303, 2003.

[7] B. Graner et al. Reduced Limit on the Permanent Electric Dipole Moment of Hg-199. *Phys. Rev. Lett.*, 116(16), Apr 2016.

[8] S.A. Murthy et al. New Limits on the Electron Electric Dipole Moment from Cesium. *Phys. Rev. Lett.*, 63(9):965, 1989.

[9] T. Chupp et al. Electric Dipole Moments of Atoms, Molecules, Nuclei, and Particles. *Phys. Rev. Lett.*, 91(1):1–15, 2019.

[10] J. Baron et al. Order of Magnitude Smaller Limit on the Electric Dipole Moment of the Electron. *Science*, 343(6168):269–272, 2014.

[11] T. Fukuyama and A.J. Silenko. Derivation of Generalized Thomas-Bargmann-Michel-Telegdi Equation for a Particle with Electric Dipole Moment. *International Journal of Modern Physics*, 28(29):135–147, 2013.

[12] E. M. Metodiev. Thomas-BMT Equation Generalized to Electric Dipole Moments and Field Gradients. *arXiv preprint arXiv:1507.04440*, 2015.

[13] J. Pretz et al. Measurement of Permanent Electric Dipole Moments of Charged Hadrons in Storage Rings. *Hyperfine Interact.*, 214(1-3):111–117, 2013.

[14] F. Rathmann et al. The Search for Electric Dipole Moments of Light Ions in Storage Rings. In *Journal of Physics: Conference Series*, volume 447, pages 11–12. IOP Publishing, 2013.

[15] A. Lehrach et al. Precursor Experiments to Search for Permanent Electric Dipole Moments (EDMs) of Protons and Deuterons at COSY. *arXiv preprint arXiv:1201.5773*, 2012.

[16] A. Lehrach et al. Design of a Prototype EDM Storage Ring. In *Proceedings, 23rd International Spin Physics Symposium: Ferrara, Italy*, pages 10–14, 2018.

[17] H. Wiedemann. *Particle Accelerator Physics*, volume 314. Springer, Cham, 2015.

[18] F. Hinterberger. *Physik der Teilchenbeschleuniger und Ionenoptik.* Springer, 2008.

[19] M.S. Rosenthal. *Experimental Benchmarking of Spin Tracking Algorithms for Electric Dipole Moment Searches at the Cooler Synchrotron COSY*. PhD thesis, RWTH Aachen U., 2016.

[20] K. Wille. *The Physics of Particle Accelerators: An Introduction.* Oxford University Press, January 2000.

[21] R. Talman. Miscellaneous Calculations for a Fully Electro-static Proton EDM Experiment, Version II. unpublished, April 2010.

[22] H. Wollnik. *Optics of Charged Particles.* Academic Press, Mar 1987.

[23] R. Baartman. Electrostatic Bender Fields, Optics, Aberrations, with Application to the Proton EDM Ring. Technical report, TRIUMF, Dec 2013.

[24] P. Grafström. Lifetime, Cross-sections and Activation. In *CERN Accelerator School, vacuum in accelerators, Platja d'Aro, Spain, 16-24 May 2006*, pages 231–226, 2007.

[25] P. Möller. Beam-Residual Gas Interactions. In *CERN Accelerator School : Vacuum Technology, Snekersten, Denmark, 28 May - 3 Jun 1999*, pages 155–164, 1999.

[26] A.F. Wrulich. Single-Beam Lifetime. In *CERN Accelerator School : 5th General Accelerator Physics Course, Jyväskylä, Finland, 7 - 18 Sep 1992*, pages 409–435, 1994.

[27] F. Hinterberger. Beam-Target Interaction and Intrabeam Scattering in the HESR Ring. Emittance, Momentum Resolution and Luminosity. Technical Report JUEL-4206, Forschungszentrum Jülich GmbH (Germany), Feb 2006.

[28] O. Boine-Frankenheim et al. Cooling equilibrium and beam loss with internal targets in high energy storage rings. *Nuclear Instruments and Methods in Physics Research Section A: Accelerators, Spectrometers, Detectors and Associated Equipment*, 560:245–255, 2006.

[29] U. Fano. Penetration of Protons, Alpha Particles and Mesons. *Annual Review of Nuclear Science*, 13(1):1–66, 1963.

[30] L. D. Landau. On the Energy Loss of Fast Particles by Ionization. *Journal of Physics (USSR)*, 8:201–205, 1944.

[31] P.V. Vavilov. Ionization Losses of High-Energy Heavy Particles. *Soviet Phys. JETP*, 5, 1957.

[32] F. Tecker. Longitudinal Beam Dynamics. In *CERN Accelerator School: Advanced Accelerator Physics Course, Trondheim, Norway, 18 - 29 Aug 2013*, pages 1–21, 2014.

[33] A. Piwinski. Intra-Beam Scattering. In *Frontiers of Particle Beams*, pages 297–309. Springer, 1988.

[34] A. Wolski. *Beam Dynamics in High Energy Particle Accelerators*. Imperial College Press, London, 2014.

[35] R.F. Carlson. Proton-Nucleus Total Reaction Cross Sections and Total Cross Sections Up to 1 GeV. *Atomic Data and Nuclear Data Tables*, 63(1):93–116, 1996.

[36] W.C. Alexander et al. *Handbook of Accelerator Physics and Engineering*. World Scientific, third edition, May 2013.

Acknowledgment

At this point I would like to thank everyone who supported me in the last year. Special thanks go to my supervisor Prof. Dr. Andreas Lehrach for the possibility to write this thesis at the Forschungszentrum Jülich and for the support in technical issues he was always willing to offer. I also would like to thank Prof. Dr. Anke Schmeink who agreed to co-supervise this thesis.

Furthermore I am grateful for all the fruitful conversations and the input I got from the members of the JEDI collaboration. The contributions in several meetings and the feedback to my results gave me a deeper inside in the whole topic of accelerator. Especially I like to mention Dr Siegfried Martin, Dr Richard M.Talman and Vera Poncza who shared their experiences in scientific working and organizational issues with me.

My final thanks go to my parents for always believing in me and all the advices and prayers they give to me.

Eidesstattliche Versicherung

Name, Vorname — Matrikelnummer

Ich versichere hiermit an Eides Statt, dass ich die vorliegende Masterarbeit mit dem Titel

Beam Simulation of a Prototype Proton Electric Dipole Moment Storage Ring

selbständig und ohne zulässige fremde Hilfe erbracht habe. Ich habe keine anderen als die angegebenen Quellen und Hilfsmittel benutzt. Für den Fall, dass die Arbeit zusätzlich auf einem Datenträger eingereicht wird, erkläre ich, dass die schriftliche und die elektronische Form vollständig übereinstimmen. Die Arbeit hat in gleicher oder ähnlicher Form noch keiner Prüfungsbehörde vorgelegen.

Ort , Datum — Unterschrift